Contrib Mineral Petrol (2008) 156:177–195
DOI 10.1007/s00410-008-0280-6

ORIGINAL PAPER

Quantifying the tectono-metamorphic evolution of pelitic rocks from a wide range of tectonic settings: mineral compositions in equilibrium

Mark J. Caddick · Alan B. Thompson

Received: 3 June 2007 / Accepted: 17 January 2008 / Published online: 5 March 2008

Abstract Commonly used thermometer and barometer calibrations are sensitive to mineral assemblage and, thus, bulk-rock composition. Calculated mineral stabilities for an average pelitic rock over a pressure–temperature (*PT*) range appropriate for normal, thickened, heated and shallowly subducted continental crust (400–900°C at 0.1–3.0 GPa) reveal more than one hundred possible assemblages. Individual phase compositions are dependent on the assemblage in which they belong and combining isopleth sets to represent $(X^{Mg}/X^{Fe})_{garnet}/(X^{Mg}/X^{Fe})_{biotite}$ and $X^{Ca}_{garnet}/X^{Ca}_{plagioclase}$ reveals several *PT*-ranges where commonly used mineral thermobarometers are less effective. For example, the garnet-biotite thermometer becomes increasingly *P* dependent in the absence of muscovite in high *T* melt-bearing assemblages, and biotite and plagioclase are not stable at pressures appropriate for lower thickened continental crust. Compositional thermobarometers involving equilibration between alternative phases (namely garnet, phengite and omphacite) are presented. Although the equilibrium compositions of phases at any *P* and *T* may change significantly as a function of bulk-rock composition, compositional-ratio thermobarometers are typically insensitive to this, unless a pseudo-univariant reaction is crossed and the buffering assemblage is altered. Quantification of the limits of efficacy of various thermobarometers allows the mineralogy of metapelites to be used to precisely determine segments of *PT* paths and infer their likely tectonic controls.

Electronic supplementary material The online version of this article (doi:10.1007/s00410-008-0280-6) contains supplementary material, which is available to authorized users.

Communicated by T. L. Grove.

M. J. Caddick (✉) · A. B. Thompson
Institute for Mineralogy and Petrology, ETH Zurich,
Clausiusstrasse 25, NW, 8092 Zurich, Switzerland
e-mail: mark.caddick@erdw.ethz.ch

Introduction

The worldwide distribution of similar metamorphic mineral assemblages in exhumed crystalline terranes supports the notion that rocks approach chemical equilibrium during regional metamorphism. Moreover, compositions of coexisting minerals show regular variation with imposed pressure (*P*) and temperature (*T*) for a given bulk-rock composition ($X_{bulk\text{-}rock}$), bulk-rock oxidation state, and sometimes fluid composition. Recent developments in petrology include comprehensive inverse methods to quantitatively evaluate parts of a rock's *PT* history from mineral assemblages and compositions. The consistency of *PT* predictions in similar tectonic settings further supports the approach to chemical equilibrium on natural metamorphic timescales, notwithstanding the fact that some minerals commonly preserve chemical zoning. It is typically presumed that *P* and *T* estimated from mineral compositions define a single equilibration point on the *PT* path followed by a rock. To ensure this is the case we must show that the apparent *P* and *T* recorded by the changing mineralogy of the rock closed to re-equilibration simultaneously. We usually have no a proiri way of knowing what deduced *P* belongs to what deduced *T*.

With the advent of internally consistent thermodynamic datasets and activity models for chemically complex minerals and natural fluids (e.g. Holland and Powell 1998; Powell and Holland 1993) it has become increasingly possible to forward-model mineral assemblage stabilities,

assigning *PT* points for the formation of metamorphic assemblages on the basis of observed mineral composition, mode, and texture (e.g. Zeh et al. 2005). For assemblages retaining obvious reaction textures and zoned minerals, it is sometimes possible to deduce several *PT* points and, thus, a small segment of the *PT* path traversed by the rock during burial and/or exhumation (e.g. Caddick et al. 2007; Harris et al. 2004). The length of the *PT* segment recoverable is, in part, dependent on the *PT*-width of the mineral stability fields traversed, differing for each diagnostic assemblage. Large regions of *PT* space are associated with common mineral assemblages which form and continue to react during metamorphism, and many smaller regions are associated with uncommon assemblages that could be produced but are likely to be subsequently destroyed. Distinguishing mineral assemblages and compositions that are uncommon as they have small *PTX* stability domains from those that are uncommon because rocks typically traverse limited parts of *PT* space is, therefore, crucial to our understanding of the evolution of metamorphic terranes, and the tectonic processes and timescales controlling this.

Our objectives here are to describe a *PT*-framework of mineral assemblages and equilibrium compositions in pelitic rocks which can illustrate the paths taken by rocks during subduction or continental collision. We (i) determine stable assemblages for average pelites at equilibrium, (ii) illustrate quantitative shifts in the apparent *P* and *T* recovered from common mineral equilibria in different bulk-rock compositions, (iii) provide alternative calibrated geothermobarometers for cases when the commonest ones are not appropriate, and (iv) describe how observed mineral compositional change reflects changes in *P* and *T* in different tectonic settings. *PT* plots contoured for equilibrium partitioning values (defined as K_D for distribution coefficients between two minerals or K_N, the equilibrium constant for a heterogeneous reaction, e.g. Ghent 1977; Thompson 1984) are shown to be robust additions to more commonly presented single-phase composition *PT* plots. This is well demonstrated by examining the sensitivity of the garnet–biotite (Gar–Bio) Fe–Mg partitioning geothermometer (e.g. Saxena 1969) to changes in bulk-rock composition (see Appendix 1 for mineral abbreviations used throughout). Against this background, disequilibrium features may be used to better understand the location and duration of the *PT* paths traversed during regional metamorphism.

Method of calculation

Mineral modes (M_{Phase}) and compositions (X_{Phase}) were calculated for an average pelite bulk-rock composition. The explored *PT* range (0.1–3 GPa, 400–900°C) encompasses most metamorphic and partial melting conditions induced in continental crust by processes involving changing crustal thickness and burial associated with subduction. The pressure range can conveniently be broken into three fields of (i) up to 1 GPa in crust of standard thickness (*ca.* 35 km Moho), (ii) 1–2 GPa in doubly thickened continental crust and upper parts of subduction zones, (iii) 2–3 GPa in super thickened continental crust and subducted continental and oceanic rocks.

Our calculations used a Holland and Powell update (2004) of their (1998) thermodynamic data-set. Free-energy minimisations with the Perplex program of Connolly (1990, 2005) utilised a newly implemented adaptive scheme of 'pseudocompound' (Connolly and Kerrick 1987) generation for phases with solid solutions. This scheme uses results of preliminary calculations to dynamically modify the compositional range and sampling density explored for each solution phase, dramatically increasing both program efficiency and the final resolution with which mineral compositions can be calculated. A resultant minimum resolution of 0.036 mol% along all solid solutions was found to be suitable for smooth contouring of mineral composition ratios. Relatively small *PT* node spacing was also required, with a final spacing of <40 bars and <1°C achieved following the method outlined by Connolly (2005). Thermobarometer calibrations are strongly dependent on the choice of mineral models used (e.g. Applegate and Hodges 1994), and these are listed in Appendix 1. Melt was modelled with the haplogranitic model of White et al. (2001). Calculations were based upon the average sub-aluminous pelite composition of (Shaw 1956) as modified by Mahar et al. (1997) to include MnO and a slightly reduced CaO content (Table 1). H_2O was considered to be in excess for sub-solidus equilibria, with supra-solidus calculations including sufficient bulk-rock H_2O to just saturate water at the solidus. This results in a small melt + H_2O field, with a low melt-fraction immediately above the solidus, and a significant increase in melt fraction as mica dehydration reactions are encountered. No additional components or phases were calculated in excess and all iron was considered as ferrous.

Assemblage stabilities under crustal conditions

Predicted stability of indicator assemblages

Figure 1 shows calculated phase assemblages for the average pelitic bulk-rock composition. Here, we briefly outline key mineral stabilities, comparing calculated equilibria with expectations from natural occurrences and experimental results.

Table 1 Average pelite composition used for calculations (modified from Mahar, et al. 1997)

	SiO_2	Al_2O_3	FeO	MgO	CaO	Na_2O	K_2O	TiO_2	MnO	Total
Weight % oxide	59.80	16.57	5.81	2.62	1.09	1.73	3.53	0.75	0.10	92.00
Molecular %	71.13	11.61	5.78	4.65	1.39	1.99	2.68	0.67	0.10	100.00
TX ranges: Mol% at $x = 0$ and $x = 1$		8.20–22.00			0.10–3.00				0.00–2.00	
Weight % oxide (Shaw 1956)	59.93	16.62	5.91	2.63	2.18	1.73	3.54	0.82	–	93.36
Weight % oxide (Symmes and Ferry 1991)	59.77	16.57	5.88	2.62	2.17	1.73	3.53	–	0.07	92.34

Row three shows *x*-axis (composition) scaling (molecular proportions) of *TX* diagrams (Figs. 5, 6, 7); rows four and five show average pelite compositions of Shaw (1956) and Symmes and Ferry (1991) for comparison

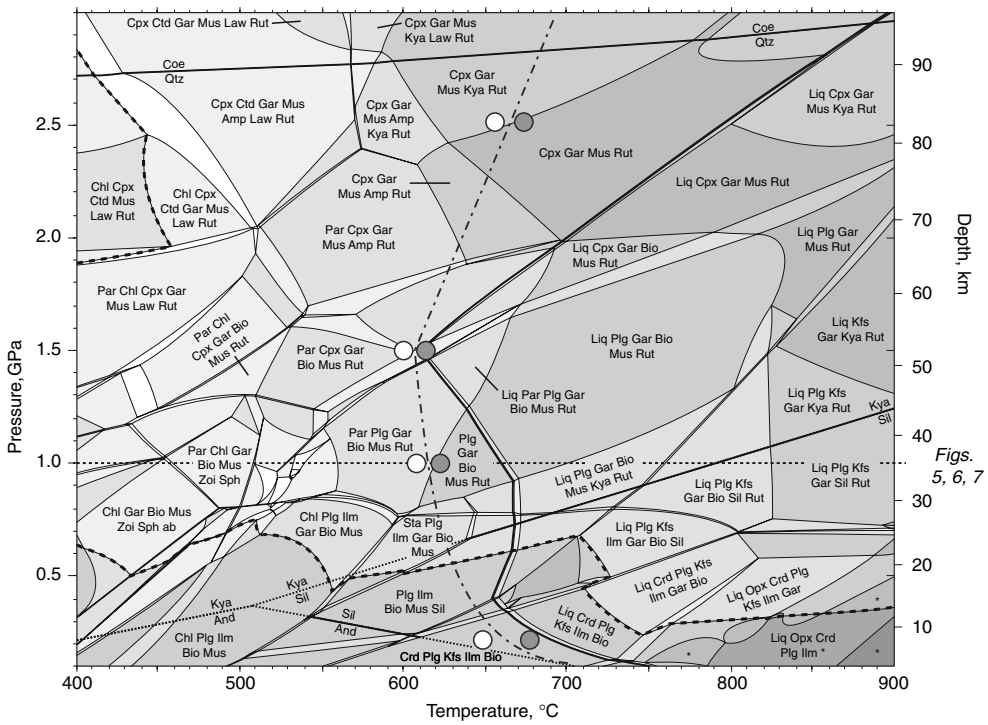

Fig. 1 *PT* stabilities of mineral assemblages for an average pelitic composition (abbreviations in Appendix 1). All fields also contain quartz or coesite, with the exception of the high *T*, low *P* fields marked with *. *Bolder curves* denote calculated quartz/coesite transition, wet melting reactions and Al_2SiO_5 phase relations (dashed in Al_2SiO_5-absent assemblage fields). *Bold dash-dotted line* from muscovite-granite melting experiments of Huang and Wyllie (1973), with *circle pairs* denoting experimental brackets. Limit of garnet stability denoted by *dashed line* at low *P* and low *T*. Depth scale calibrated by calculating bulk-rock densities along a 600°C section. 1 GPa (*ca.* 35 km depth) section appropriate for Figs. 5, 6, 7 is also shown. Variance ($\omega = c + 2 - \phi$) increases from *white* to *dark shading*, typically increasing towards higher temperature and lower pressure as solid solutions become more extensive

Continental crust of standard thickness

Phase equilibria in the 0.1–1 GPa range have become well known (e.g. Powell and Holland 1990; Spear and Cheney 1989; Thompson 1976) as they predict common regional metamorphic progressions. The dominant reactions are based in the KFMASH sub-system, hence the success of the AFM-projection for metapelites (Thompson 1957). It is clear that the most commonly observed pelitic mineral assemblages occupy the largest *PT* stability fields (Fig. 1). Recognition of stable assemblages with more limited *PT* stabilities would be diagnostic of short segments of *PT* paths, and identification of replacement assemblages suggests the orientations of *PT* path segments followed.

Extension from KFMASH to a CaO, Na_2O, MnO, and TiO_2-bearing system allows consideration of accessory phases, haplogranitic melt, and key equilibria at higher pressure. Our calculations predict a feldspar-bearing Barrovian sequence terminated by mid-crustal wet melting at *ca.* 650°C and pressure-increasing muscovite-dehydration between 550°C (0.1 GPa) and 750°C (1 GPa). The calculated wet solidus agrees well with experimental constraints (e.g. Huang and Wyllie 1973) below 0.4 GPa and at *ca.* 1.5 GPa, with a large jump in melt fraction at the

muscovite-out reactions, coincident with Kfs-in and consistent with field and experimental data (e.g. Gardien et al. 1995). Calculated melts coexist with assemblages typical of migmatitic restites (e.g. Kriegsman 2001).

Low-temperature topologies in Fig. 1 appear to be dramatically different from previous KFMASH and MnKFMASH calculations (e.g. Mahar et al. 1997; Powell et al. 1998; Xu et al. 1994), but this is primarily due to superimposed 'accessory phase' reactions. Significant examples include termination of the approximately isobaric (*ca*. 0.8 GPa) rutile–ilmenite transition at *ca*. 530°C, which stabilises titanite at lower temperatures. Additional detail unique to the Na + Ca system comes from breakdown of plagioclase to zoisite and end-member albite, and the stabilities of paragonite and clinopyroxene.

Thickened continental and subducted crust

The dominant feature of the 1–2 GPa range is the amphibolite–eclogite transition above *ca*. 550°C. This coincides with experimental determinations of albite breakdown to jadeite + quartz (Holland 1980; Johannes et al. 1971; Newton and Smith 1967) and is responsible for a significant inflexion in the wet solidus. The calculated solidus, which agrees well with experimental brackets up to the plagioclase–clinopyroxene transition, subsequently has a positive d*P*/d*T* at higher pressures and occurs at progressively higher temperatures than determined experimentally (*ca*. 200°C higher at 3 GPa). Several reasons for these discrepancies at high *P* are described elsewhere (Holland and Powell 2001). We note here, however, that additional calculations of mineral and melt modes and compositions at high *T* and low bulk-rock H_2O content are reasonably consistent with the results of mica-dehydration experiments up to at least 2 GPa (unpublished results).

The most significant feature of Fig. 1 at 2–3 GPa is the transition from blueschist-type to eclogite-type assemblages with increasing temperature. However, although the mineral assemblage changes significantly over the temperature range of interest, abundances of the three dominant phases (phengite *ca*. 35 vol%, omphacite *ca*. 10%, and quartz *ca*. 35%) remain similar over a large temperature range. A more readily observable change is that chloritoid (≤12 vol%) and the small amounts of chlorite (≤4%), lawsonite (≤6%), and glaucophane (≤8%) stable at low *T* are progressively lost upon heating, resulting in garnet growth (reaching *ca*. 16 vol% at 750°C). Systematic changes in the compositions of the major phases indicate their potential utility as thermobarometers, and we calibrate expressions for some of these later.

Mineral equilibria at high pressure are particularly bulk-rock composition sensitive, with carpholite-bearing assemblages and talc + kyanite white schists stabilised by higher bulk-rock Al and Mg contents (Wei and Powell 2003, 2004). We do not explore these compositions further here.

The stability of commonly used thermobarometers

Calibrations of Gar–Bio and Gar–Plg (+ Al_2SiO_5 + SiO_2) thermobarometers are frequently used to determine the conditions of equilibration of metapelitic rocks. We extracted phase compositions from the Perplex output used to generate Fig. 1, calculating K_D and K_N ratios appropriate to the thermobarometers and contouring in *P* and *T* with a simple Matlab script.[1] The results visually represent the calculated response of K_D and K_N to pressure, temperature, and mineral assemblage. Furthermore, the role of seemingly minor components on the stability and compositions of phases can be explored, and the *PT* stability limits of each buffered assemblage quantified.

The Fe/Mg garnet–biotite exchange thermometer

For the average pelitic composition, the Gar–Bio assemblage has an extensive stability field from <400°C to *ca*. 820°C and *ca*. 0.3–2.0 GPa (Fig. 2a). The lower and upper pressure limits of this field are defined by the absolute garnet and biotite stabilities, respectively, and the upper temperature limit is defined by the melting of biotite assemblages. Garnet stability limits are particularly sensitive to bulk-rock Mn content (Mahar 1997), with strong partitioning of Mn into garnet at low M_{Gar}, demonstrated below and in Fig. 7. Reactions at the limits of the Gar-Bio bearing *PT* field are listed in Fig. 2a.

Equilibrium phase compositions were combined in the expression $[K_D]^{Mg}_{Fe\,Gar\,Bio} = (X^{Mg}/X^{Fe})_{Gar}/(X^{Mg}/X^{Fe})_{Bio}$, with mole fraction terms defined as $X^{Mg}_{Gar} = (Mg/[Mg + Fe + Ca + Mn])_{Gar}$ and $X^{Mg}_{Bio} = (Mg/[Mg + Fe + Mn])_{Bio}$. Figure 2a is contoured with iso-$[K_D]^{Mg}_{Fe\,Gar\,Bio}$ lines, effectively showing the basis of thermometer calibrations expressed in a form that is relatively independent of bulk-rock composition (as demonstrated in Figs. 5, 6, 7). In general, we obtain-$[K_D]^{Mg}_{Fe\,Gar\,Bio}$ values very close to previous calculations (e.g. Thompson 1984, p. 182) for the *PT* range appropriate for Barrovian regional metamorphism, although several complexities are observed. Given these calculations it is possible to re-fit a simple thermometer expression with a

[1] Script available for download from http://www.perplex.ethz.ch/perplex/ibm_and_mac_archives/matlab_plotting_scripts.zip.

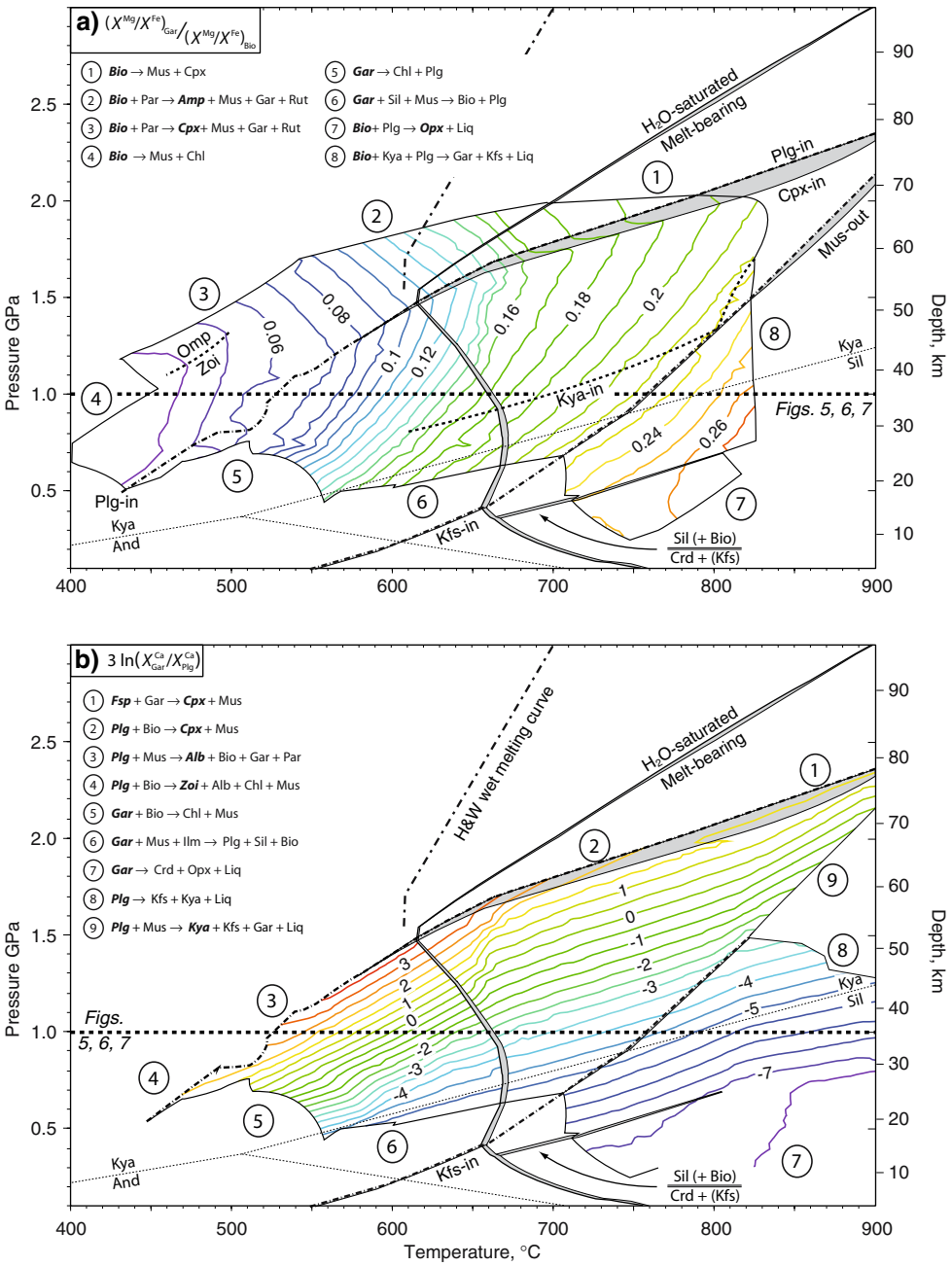

Fig. 2 *PT* extents and equilibrium partitioning values of the most commonly used metapelite mineral thermometer (**a** $[K_D]^{Mg}_{Fe\,Gar\,Bio}$) and barometer (**b** $[K_N]^{Ca}_{Gar\,Plg}$), with buffering assemblages as in Fig. 1. Several key equilibria are also shown. Gar + Bio and Gar + Plg stability fields are limited by numbered reactions describing the phases produced when these phases are lost. Reactions are written here schematically assuming SiO_2 and H_2O in excess. *Bold-italicised phases* are only stable on one side of the reaction, the modes of other phases change across the reaction, but do not reach zero. To give constant isoline spacing (**b**) is plotted as ln K_N. See Appendix 1 for mineral abbreviations

multiple linear regression through the contoured data surface of Fig. 2a:

$$T(^{\circ}\mathrm{C}) = 1504.21[K_D]^{Mg}_{Fe\,Gar\,Bio} + 73.6P(\mathrm{GPa}) + 335.6 \qquad (1)$$

for which R^2 of the fit is 0.96.

$[K_D]^{Mg}_{Fe\,Gar\,Bio}$ isoline slopes can clearly be deflected by changing the buffering assemblage, and Fig. 2a can be used to estimate where these displacements occur. $[K_D]^{Mg}_{Fe\,Gar\,Bio}$ contours fall into two domains, with positive dP/dT (*ca.* 10 MPa°C^{-1}) in low pressure plagioclase-bearing fields and negative dP/dT in higher pressure, omphacite-bearing (plagioclase-absent) fields. The sharp transition in isoline slopes between the domains shows that the presence of these phases significantly influences the modelled K_D equilibria, which is not dramatically deflected by other low T-assemblage boundaries. Although $[K_D]^{Mg}_{Fe\,Gar\,Bio}$ isolines are generally steep in supra-solidus fields, they are curved, becoming shallower at lower pressures than the kyanite-in curve (between 0.9 and 1.4 MPa), in the assemblage melt + Kya + Plg + Gar + Bio + Mus + Rut + Qtz. $[K_D]^{Mg}_{Fe\,Gar\,Bio}$ contours have a significant P dependence in muscovite-absent fields and are further deflected by the Crd-in reaction.

To summarise, $[K_D]^{Mg}_{Fe\ Gar\ Bio}$ isoline contours to fall into three principle *PT* regions; d*P*/d*T* is steeply negative in the presence of omphacite (high *P* and low *T*), is steeply positive in the presence of plagioclase and muscovite ('Barrovian' *PT*s), and is positive but shallower at low *P* (at low garnet abundance and in the absence of muscovite). These changes principally reflect non-ideal grossular and Tschermak interactions in the garnet and biotite solution models, respectively, with both interactions becoming increasingly significant as the phases move away from Fe–Mg binaries towards their stability limits. Combining all of the K_D-isoline deflections into two correction factors gives an alternative equation best-fit equation:

$$T(^\circ\mathrm{C}) = 1881.2[K_D]^{Mg}_{Fe\ Gar\ Bio} + 60.6P(\mathrm{GPa}) + 259.6X^{gro}_{Gar} - 183.4X^{spe}_{Gar} + 258.3 \quad (2)$$

in which R^2 is 0.98. Correction factors X^{gro}_{Gar} and X^{spe}_{Gar} allow the thermometer to successfully predict temperature at both the *PT* extremes of Gar–Bio stability (as the phases deviate significantly from almandine-pyrope and phlogopite-annite binaries), and in bulk-rock compositions that differ from our calculation. The resulting expression retrieves similar temperatures to the Ferry and Spear (1978) thermometer at low pressure, with increasing deviation from their result at high pressure principally reflecting the shift of garnet towards grossular (see Appendix 2 for comparisons of our thermobarometers with others from the literature). The general utility of Gar–Bio thermometry in rocks of other bulk-rock composition is described later.

Ca partitioning between garnet and plagioclase

The garnet-plagioclase (GASP) mineral barometer (Ghent 1976; Hodges and Spear 1982; Newton and Haselton 1981; Tracy et al. 1976) uses the end member reaction

$$3\ CaAl_2Si_2O_8(ano) = Ca_3Al_2Si_3O_{12}(gro) + 2\ Al_2SiO_5(Kya) + SiO_2(Qtz) \quad (3)$$

as a reference. However, in quartz-bearing assemblages any other mineral combination that buffers Al_2O_3 provides a potential garnet + plagioclase thermobarometer, relative to the compositional part of the equilibrium constant. Garnet and plagioclase are stable, up to pressures that define the eclogite facies, where plagioclase breakdown forms pyroxene along reactions labelled 1 and 2 in Fig. 2b. The lower pressure limit of GASP assemblages is the garnet-out reaction (5 to 7 in Fig. 2b).

Calculated iso-lines for $[K_N]^{Ca}_{Gar\ Plg} = \left(X^{Ca}_{Gar}\right)^3 / \left(X^{Ca}_{Plg}\right)^3$ are shallow across most of the examined *PT* space (d*P*/d*T* = 2 to 4 MPa°C^{-1}, Fig. 2b); hence the usefulness of the expression as a barometer. Contours show far less dependency on the various buffering assemblages than does the $[K_D]^{Mg}_{Fe\ Gar\ Bio}$ thermometer, although the K_N-isolines clearly steepen in paragonite-bearing fields. Additionally, $[K_N]^{Ca}_{Gar\ Plg}$ isoline distribution is not constant over *PT* space (note that Fig. 2b is plotted as ln K_N), with increasing contour density towards higher pressure reflecting the exponential dependence of the equilibrium constant upon $\Delta G_{reaction}$. We find good agreement (typically within one *ln* unit) with earlier predictions (e.g. Thompson 1984) in the range 0.5–1.0 GPa, 500–700°C.

Regression through the contoured data (Fig. 2b) yields the barometer expression

$$P(\mathrm{GPa}) = [(0.00259 - 0.000313z) \times T(\mathrm{K})] + \left[\ln [K_N]^{Ca}_{Gar\ Plg} \times (0.171 - 0.0763z)\right] - 0.991 \quad (4)$$

in which $[K_N]^{Ca}_{Gar\ Plg}$ is defined as $\left(X^{Ca}_{Gar}\right)^3 / \left(X^{Ca}_{Plg}\right)^3$, z has a value of 1 or 0 in paragonite-bearing or absent assemblages, respectively, and $R^2 = 0.95$. z compensates for changes in the assemblage buffering of Na which modify X^{alb}_{Plg} (and hence X^{ano}_{Plg}) and introduce curvature to K_N contours. Calibration (4) agrees well with that of Hodges and Spear (1982) except at high *P*, low *T*, and at $T > 850$°C, where results of the two calibrations differ by up to 0.3 GPa (Appendix 2).

Deducing tectonic histories from metamorphosed continental crust

Co-existing mineral compositions are typically considered to record selected points along the *PT*-paths experienced during orogenesis, so it is instructive to compare the *PT* locations of such paths in terms of the various thermobarometric methods used. *PT* paths from the literature, deduced from multiple recorded equilibria in metamorphic mineral assemblages, are presented against the background of the $[K_D]^{Mg}_{Fe\ Gar\ Bio}$ thermometer and the GASP $[K_N]^{Ca}_{Gar\ Plg}$ geobarometer (Figs. 3a, b). These examples and aspects of their deduction are briefly described here.

Barrovian type regional metamorphism

Mid- and lower-crustal thickening are typified by burial to *ca.* 0.5–1.2 GPa (*ca.* 20–40 km), followed by heating towards or through the wet-solidus and subsequent exhumation into the brittle-regime (e.g. the High Himalayan Crystalline Sequence, path HH in Fig. 3). Such *PT*

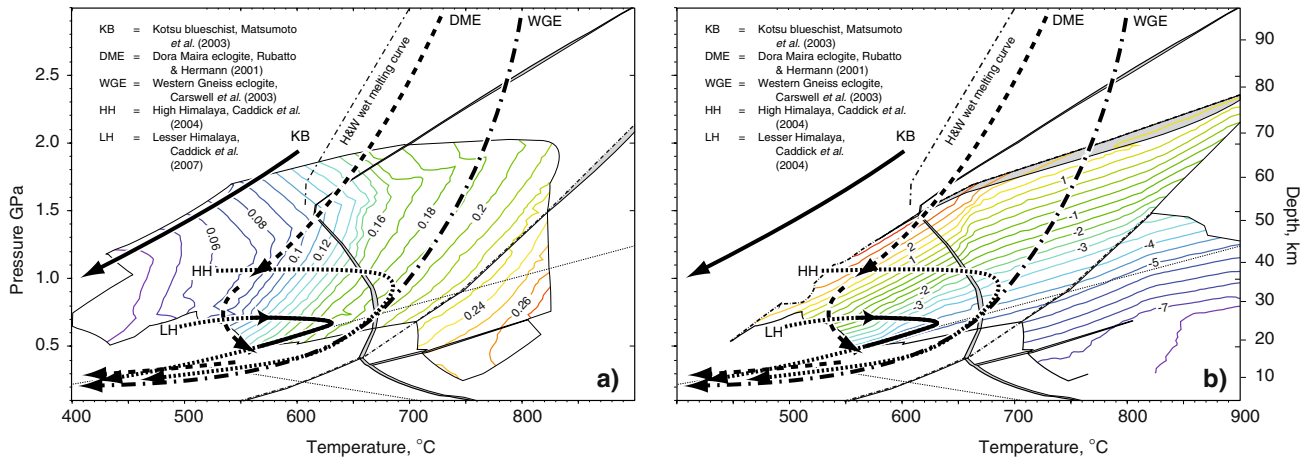

Fig. 3 Relationships between *PT* paths experienced by rocks from a variety of tectonic settings and the **a** Gar–Bio and **b** Gar–Plg thermobarometers. Regional crustal thickening producing 'Barrovian style' metamorphism is represented by the High Himalayan path (HH), very rapid tectonic burial and exhumation is represented by the Lesser Himalaya (LH) and subduction-related processes are represented by blueschist (KB) and eclogite (DME and WGE) paths. Burial paths from high-*P* rocks are petrographically difficult to decipher because of near-peak *T* overprinting and are, consequently, not shown. The deeply buried rocks only enter Gar–Bio–Plg bearing stability fields during exhumation. Exhumation paths of the eclogite samples (DME and WGE) are sub-parallel to $[K_D]^{Mg}_{Fe\ Gar\ Bio}$ isopleths along much of their history, but experience a steady decrease in $[K_N]^{Ca}_{Gar\ Plg}$

histories are typically constructed from two or three points corresponding to distinct mineral compositions and textures. Where possible, these partial paths are constrained from single samples which can subsequently be compared across the terrane (e.g. Caddick, et al. 2004). In the absence of evidence for compositional resetting (e.g. Florence and Spear 1991) the highest temperature recorded by the $[K_D]^{Mg}_{Fe\ Gar\ Bio}$ thermometer is commonly considered to represent the highest temperature point experienced by the rock, although this can clearly be lost during cooling of high-grade samples (Vannay and Grasemann 1998). Placing barometry results into tectonic context is more difficult, involving a decision as to whether equilibria refer to the point of maximum *P*, the *P* at maximum *T*, or some intermediate point. Textural features related to decompression, such as the partial breakdown of garnet to form plagioclase, can be combined with garnet-zoning patterns to determine whether barometric results represent P_{Max} or some other pressure on the *PT* path.

Obvious evidence of the earliest segment (prograde path) is commonly difficult to find preserved, as the assumption of continued equilibration implies that textures and compositions will be progressively overprinted during heating. Retention of prograde mineral compositions is a function of both thermal history and the size of crystals preserved, with high *T* and small crystal sizes favouring overprinting. Nonetheless, zoned plagioclase and garnet, and inclusions within these phases may reveal parts of the pre-peak history, and changing compositions from crystal cores to rims can suggest the relative d*P*/d*T* experienced during burial (e.g. Spear et al. 1984). This identification of zoning 'orientation' is important, as Fig. 2a highlights that any given $[K_D]^{Mg}_{Fe\ Gar\ Bio}$ value will occur twice during the history of a rock (upon heating and then during cooling).

PT constraints along the exhumation (and cooling) path include calibrations of retrograde features (e.g. chlorite-in) and can be dated relatively by modelling closure temperatures of mineral geochronometers. Although temperature–chronology data from the exhumation path can be combined, the depth to which they refer is often retrieved by exhumation modelling rather than direct petrological techniques.

The d*P*/d*T* of exhumation paths is probably controlled by overthrusting, extensional thinning, and erosion. Depending on exhumation rate and heat supply, this can include additional heating (England and Thompson 1984), possibly leading to anatexis upon mica breakdown (e.g. Storre and Karotke 1972). Crucially, however, without an additional heat source (i.e. no asthenospheric proximity or contact with mafic magma) these rocks will spend much of their history in garnet–biotite and garnet–plagioclase assemblage stability fields. Average pelitic rocks following such paths consequently experience 'Barrovian style' mineral progressions, although only small parts of the sequence will be preserved in any one sample. In the case of path HH, this is recorded as peak kyanite + garnet ± sillimanite ± melt stability, as seen from overlaying the *PT* path in Fig. 3 onto Fig. 1. Contrasting mineral assemblages, compositions, and zoning in many ostensibly similar rocks can be used to reveal quite different depths of

burial, maximum temperatures and, by inference, tectonic histories (e.g. path LH, Caddick et al. 2007).

Exhumation of deeply buried or subducted continental crust

Several recently described *PT* paths reflect deep burial or subduction of continental rocks to >100 km followed by rapid exhumation back to the surface (e.g. the Kotsu Blueschists, Dora Maira Eclogite, and Western Gneiss Eclogite, Fig. 3). Exhumation from depths of more than 100 km cannot be principally steered by surface erosion and must involve extrusion within the orogen, possibly involving buoyant flow back up the subduction channel (e.g. England and Holland 1979), and requiring either extension or thrusting coupled with erosion (Maruyama et al. 1994; Okay et al. 1993). The density contrast between the subducted continental crust and the mantle implies that exhumation of ultrahigh-pressure terranes is likely to operate in at least two stages (e.g. sub-horizontal extension and vertical doming following a phase of sub-horizontal shortening and vertical extrusion and erosion, Hacker et al. 1995).

The *PT* histories illustrated in Fig. 3 carried high-pressure assemblages through at least 50 km of crust with, in some cases, insufficient retrograde re-equilibration to frustrate peak-*PT* thermobarometry. In many cases, however, ultrahigh-pressure rocks preserve evidence of their deep burial only as isolated indicator inclusions (e.g. coesite, diamond or pseudomorphs thereafter) within refractory crystals. Accurate assessment of burial conditions requires both primary equilibration and subsequent retention of mineral assemblage and phase compositions during exhumation. Gar + Bio + Plg stabilities are exceeded under these conditions (Fig. 1) so alternative thermobarometers are required, with Gar + Omp assemblages permitting thermometry (e.g. Ellis and Green 1979) and the celadonite component in white-mica recording pressure dependence (e.g. Massonne and Schreyer 1987). These equilibria are discussed later.

Deduced exhumation paths from most eclogites typically entail coupled cooling and decompression from the point of maximum burial. Whether this is a primary result of exhumation mechanisms is uncertain because unless heat is efficiently lost from the rising eclogite, mineralogical evidence of the highest pressures will be lost via overprinting (Ernst 2006). This leads to a pre-disposition to preserve some *PT* path types whilst destroying evidence of others, and may explain why most deduced exhumation paths are sub-parallel to Gar–Bio isoline sets (e.g. Fig. 3). Preservation potential can be usefully quantified with reference to fluid availability during exhumation, as heating typically liberates fluid from any remaining hydrous phases whilst cooling paths usually require externally derived fluids for reactions to progress. For instance our calculated average metapelite would require up to 1.8 wt% additional H_2O to fully equilibrate retrogressive hydrous phases if undergoing the Dora Maira exhumation path of Rubatto and Hermann (2001). In the absence of externally derived fluids the rock would essentially be 'fluid deficient' during decompression until it reached the inferred heating phase between 0.9 and 0.5 GPa, and re-equilibration until this point would be limited.

Plagioclase growth during exhumation of kyanite + quartz eclogites permits GASP geobarometry, but equilibria probably record a wide range of pressures partly limited by kinetic controls on crystal nucleation and growth. Given the interest in constraining exhumation rates of high- and ultrahigh-pressure eclogites, it is important to know whether a pressure retrieved by mineral-composition barometry actually records the maximum burial depth, some point along the exhumation path, or some other, unrelated point in *PT* space. Such inferences are currently difficult to make in many circumstances, as nucleation-growth-diffusion rates are still relatively poorly constrained at appropriate *PT* conditions.

Geothermobarometers for average pelite at high pressures

Mineral assemblages with small *PT* stability fields (e.g. Law + Chl + Ctd or Law + Kya) can closely reveal the *PT* of equilibration (Fig. 1). Within larger assemblage fields mineral compositional variability can be used, and here we examine high *P* phase compositions, briefly reviewing potential thermobarometers for common assemblages. In particular, at pressures > 2 GPa, assemblages containing garnet + omphacite + phengite are prevalent and extend over wide regions of *PT* space (Fig. 1) Their calculated compositional variation has been calibrated in terms of four thermobarometric expressions.

Garnet–Phengite thermometry

Phengite is an important phase in high-pressure pelitic rocks, partitioning Fe and Mg into its M sites and providing a possible exchange thermometer with garnet (e.g. Green and Hellman 1982). To examine this we have contoured coexisting garnet–phengite compositions with the expression $K_D = (X^{Mg}/X^{Fe})_{Gar}/(X^{Mg}/X^{Fe})_{Phe}$, where X^{Mg}_{Gar} follows the Gar–Bio example and $X^{Mg}_{Phe} = (Mg/[Mg +$

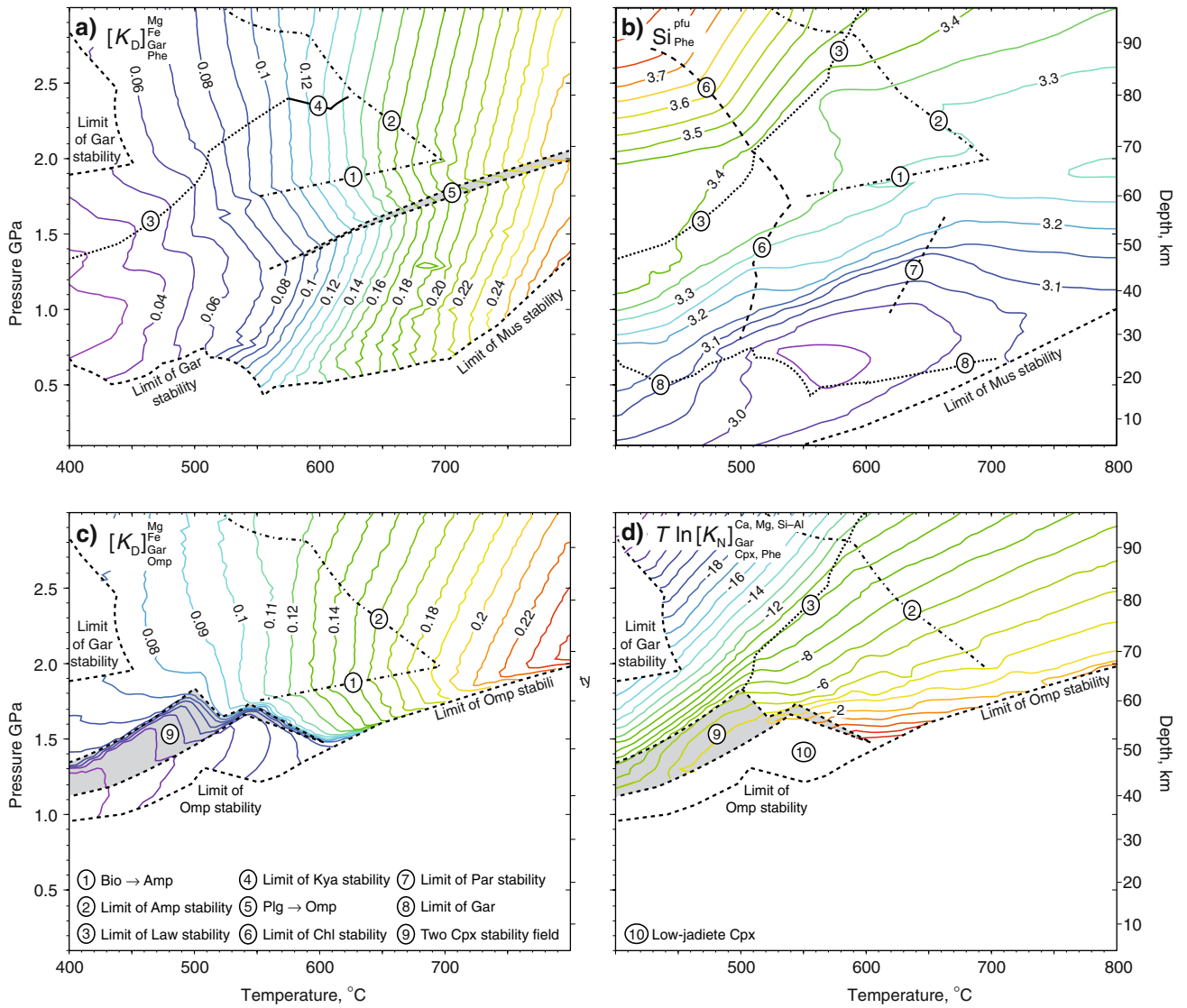

Fig. 4 *PT* calibrations of selected K_D, K_N and compositional isolines for high *P* equilibria involving garnet, omphacite and phengite, calculated from Perplex data used to construct Fig. 1. Contours show **a** $[K_D]^{Mg}_{Fe\ Gar\ Phe}$, **b** Si^{pfu}_{Phe}, **c** $[K_D]^{Mg}_{Fe\ Gar\ Omp}$ and **d** $\left(T \ln[K_N]^{Ca,Mg,Si-Al}_{Gar\ Cpx,Phe}\right)/1000$, with the equilibrium coefficient as defined in the text. Key mineral assemblage limits are shown by *numbered curves* and are taken from Fig. 1. *Shaded fields* in **c**, **d** show a region of two coexisting pyroxenes

Fe])$_{Phe}$. The result (Fig. 4a) demonstrates the applicability of this expression as a thermometer over a very wide range of *PT* space, including a region at *ca.* 0.5–2.0 GPa that overlaps with the Gar–Bio thermometer. $[K_D]^{Mg}_{Fe\ Gar\ Phe}$ increases between 400 and 800°C, with isoline deflections coinciding with the Plg–Omp transition (reflecting the incorporation of Fe–Mg into the omphacite structure and a dramatic change in X^{gro}_{Gar}), the breakdown of biotite at 1.5–2.0 GPa, the upper limit of amphibole stability, and the incoming of high-*P* lawsonite or kyanite. A best-fit equation to the garnet–phengite data gives a simple thermometer expression:

$$T(^\circ\mathrm{C}) = 176.6 \ln[K_D]^{Mg}_{Fe\ Gar\ Phe} - 7.07P(\mathrm{GPa}) + 1002.7 \quad (5)$$

where $R^2 = 0.93$. Although the fit is good, addition of a grossular correction accounts for some of the K_D-isoline deflection associated with Plg-out, increasing the efficacy of the expression over a wide *PT* range:

$$T(^\circ\mathrm{C}) = 218.6 \ln[K_D]^{Mg}_{Fe\ Gar\ Bio} + 11.51P(\mathrm{GPa}) + 328.5X^{gro}_{Gar} + 1009.9 \quad (6)$$

where $R^2 = 0.98$. Expression (6) recovers *T* to within *ca.* 35°C of the original Perplex output over the entire *PT* range. Retrieved temperatures are typically lower than

those from the Green and Hellman (1982) Gar–Phe thermometer (Appendix 2), agreeing well with that of Wu et al. (2002).

Phengite composition barometry

The pressure dependence of white-mica Si-content is well established (e.g. Massonne and Schreyer 1987). Our use of the Coggon and Holland (2002) phengite model reveals a strong correlation between pressure and Si-content, and a weaker negative correlation between temperature and Si-content. This results in variation between *ca.* 3 and 3.8 atoms per formula unit (Si^{pfu}_{Phe}) over the examined *PT* range (Fig. 4b), with temperature dependence of Si^{pfu}_{Phe} most pronounced near the limits of lawsonite stability in the absence of chlorite and at pressures below *ca.* 1.2 GPa. Calculated coexisting garnet compositions are in the range $X^{alm}_{Gar} = 0.62 - 0.96$, with phengite compositions falling between experimental phengite + garnet + kyanite + quartz determinations in KMASH and KFASH (Massonne and Szpurka 1997). Testing of the phengite model in numerous subsystems (KFASH, KMASH, NKASH, and NKMASH) was discussed by Coggon and Holland (2002). Regression of our data (Fig. 4b) yields the simple barometer expression

$$P(\mathrm{GPa}) = 4.19\mathrm{Si}^{pfu}_{Phe} + 0.0036T(\mathrm{K}) - 15.15 \quad (7)$$

for which $R^2 = 0.77$. Because Si increase (from *ca.* 3–3.8 apfu) in phengite is primarily through a Tschermak ([Mg,Fe]Si $\rightleftharpoons$ AlAl) exchange, Mg content is also strongly *PT* dependent (increasing from *ca.* 0–0.5 apfu over the same *PT* range). Coupled regression of Si^{pfu}_{Phe} and Mg^{pfu}_{Phe} values gives the expression:

$$P(\mathrm{GPa}) = 8.35\mathrm{Mg}^{pfu}_{Phe} - 1.72\mathrm{Si}^{pfu}_{Phe} + 0.0015T(\mathrm{K}) + 4.59 \quad (8)$$

With an R^2 of 0.90. Fe^{pfu}_{Phe} was found to be far more temperature dependent than Mg^{pfu}_{Phe}, hence the use of the latter here and the ratio between both in thermometer calibrations (5–6). Use of calibration (8) yields pressures to within 0.4 GPa of the original output data from the free-energy minimisation, with maximum deviation at the lower pressure stability limit of white-mica. It also compares well with experimental constraints (Appendix 2).

Garnet–Omphacite thermometry

Fe–Mg exchange between numerous high pressure (e.g. amphibole, chlorite, and chloritoid) phases provides potential thermometers, but for the bulk composition of interest, garnet and omphacite are stable over the widest *PT* range of any pair other than garnet–phengite, and the modal proportion of each phase is well above the percent level for most of this *PT* window. Calculated $[K_D]^{Mg}_{Fe\ Gar\ Omp}$ is highly temperature dependent (Fig. 4c), increasing continually over the range 450–800°C. Minor isoline deflections occur at the limits of amphibole stability and in a 2-Cpx field at *ca.* 1.5 GPa, 500°C. The contoured data can be regressed to give the expression

$$T(^\circ\mathrm{C}) = 294.2\ln[K_D]^{Mg}_{Fe\ Gar\ Omp} + 28.6P(\mathrm{GPa}) + 416.3X^{gro}_{Gar} + 1098.7 \quad (9)$$

where $R^2 = 0.98$. This expression is effective as a thermometer in the pressure range 1.5–3 GPa, yielding temperatures within 35°C of the Perplex output over all of the 1-Cpx stability range and within 15°C for most of that range (Appendix 2). Retrieved temperatures are within the range given by the various Gar–Omp thermometer calibrations collated by Ravna (2000) at 3.2 GPa, and 18–70°C lower at 1 GPa. (Appendix 2).

Garnet–Omphacite–Phengite barometry

The replacement of plagioclase by clinopyroxene at high pressure results in a garnet, omphacite, and phengite geobarometer for eclogites. The equilibria, as outlined by Waters and Martin (1993), involves diopside formation at the expense of garnet:

$$\mathrm{Mg_3Al_2Si_3O_{12}(pyr)} + 2\ \mathrm{Ca_3Al_2Si_3O_{12}(gro)} = 6\ \mathrm{CaMgSi_2O_6(dio)} + 3\ \mathrm{Al_2Mg_{-1}Si_{-1}} \quad (10)$$

where the final term represents Tschermak exchange in muscovite–phengite. We have extracted mineral site occupancies from the data used to generate Fig. 1, combining them into an equilibrium constant which, following Waters and Martin (1993), is defined as:

$$[K_N]^{Ca,Mg,Si-Al}_{Gar\ Cpx,Phe} = 6\ln a_{dio} - \ln a_{pyr} - 2\ln a_{gro} + 3\ln\left(\frac{X^{Al}_{M1}X^{Al}_{T2}}{X^{Mg}_{M1}X^{Si}_{T2}}\right)_{Phe} \quad (11)$$

Figure 4d shows contours representing $T\ln[K_N]^{Ca,Mg,Si-Al}_{Gar\ Cpx,Phe}$, demonstrating the general applicability of the equilibria as a geobarometer. $T\ln[K_N]^{Ca,Mg,Si-Al}_{Gar\ Cpx,Phe}$ decreases steadily towards higher pressure, with few deflections associated with changing mineral assemblage except for an increased temperature-dependence in low-*T* lawsonite and amphibole-bearing fields. Regression of the data in Fig. 4d gives a simple barometer expression:

$$P(\mathrm{GPa}) = 0.00311T(\mathrm{K}) - 0.000126T \ln [K_N]^{Ca,Mg,Si-Al}_{Gar\ Cpx,Phe} - 1.36 \quad (12)$$

for which $R^2 = 0.91$. An alternative expression accounts for the stability of lawsonite at low temperature and the resultant steepening in isoline gradients:

$$P(\mathrm{GPa}) = \left[(0.0000314l - 0.000150)T(\mathrm{K}) \ln [K_N]^{Ca,Mg,Si-Al}_{Gar\ Cpx,Phe}\right] + [(0.00272 + 0.000136l)T] - 1.12 \quad (13)$$

where $l = 1$ in lawsonite-bearing assemblages and $l = 0$ in the absence of lawsonite. This expression (with an R^2 of 0.93) yields pressures within 0.4 GPa of the input data over the entire *PT* range of its calibration. It can be coupled with Fe–Mg exchange thermometers (Eqs. 6, 9) to give a consistent set of *PT* estimates for Gar–Omp–Phe-bearing eclogite rocks.

Sensitivity of mineral compositions to changes in bulk-rock composition

Mineral stabilities and co-existing compositions have been determined for an average pelitic rock over a wide range of *P* and *T*. It is important, however, to know whether the most commonly used mineral thermobarometers are equally effective for *all* pelitic rock compositions, and to understand any systematic variations in their behaviour as a function of bulk-rock composition. Determination of the compositional domains outside which certain thermobarometers are ineffective is important because a wide variety of protolith compositions may develop 'pelitic' mineral assemblages and metasomatic processes may modify the compositions of such rocks during orogenesis.

Gar + Bio coexist with many different phases depending upon rock composition and *PT*. Because $[K_D]^{Mg}_{Fe\ Gar\ Bio}$ records simple cation exchange it should be relatively continuous across *PT* regions containing a sequence of additional phases. However, as demonstrated above, non-ideal interactions with additional components can affect K_D-isolines, particularly if the buffering assemblage is changed. Here we examine the effect of changing bulk-rock composition on calculated $[K_D]^{Mg}_{Fe\ Gar\ Bio}$ and $[K_N]^{Ca}_{Gar\ Plg}$ for cases in which the buffering assemblage remains constant and cases in which it is changed. Bulk-rock Al_2O_3 and CaO variation were chosen to demonstrate the response of K_D and K_N to changing major bulk-rock components. MnO demonstrates the importance of a common 'minor component' that fractionates much more strongly into one of the thermobarometer phases than the other. Bulk-rock FeO and MgO variation is not shown because its consequences are readily determined by tie-lines in available AFM compatibility diagrams and TX plots (e.g. Spear and Cheney 1989; Thompson 1976).

Al_2O_3 variation

Bulk-rock Al_2O_3 content controls the relative stabilities of numerous metapelite minerals, particularly at pressures above plagioclase and biotite-out. $T - X^{Al_2O_3}_{bulk-rock}$ diagrams demonstrate the relationship between bulk-rock Al content and the abundances and compositions of Gar and Bio at 1.0 GPa (Fig. 5), with *x* axes corresponding to Al_2O_3 contents between 8.2 mol% (at $x = 0$) and 22.0 mol% (at $x = 1$).

At relatively low $X^{Al_2O_3}_{bulk-rock}$ and temperatures above *ca.* 530°C, kyanite and paragonite are absent and the modal proportions of garnet and biotite (M_{Gar} and M_{Bio}, Fig. 5a, b) are directly controlled by bulk-rock Al_2O_3 content. At higher $X^{Al_2O_3}_{bulk-rock}$, Al_2O_3 is effectively buffered by an additional phase, with the slopes of Kya-in, Par-in, Plg-in, Chl-in, and Bio-in all showing both *T* and $X^{Al_2O_3}_{bulk-rock}$ dependence. In the presence of one of these buffers, M_{Gar} is controlled primarily by bulk-rock FeO. X^{alm}_{Gar} isopleths are sub-parallel to M_{Gar} (Fig. 5a–c), showing strong $X^{Al_2O_3}_{bulk-rock}$ dependency in the absence of Kya, Par, Plg or Chl. X^{gro}_{Gar} (Fig. 5c) is negatively correlated with X^{alm}_{Gar}, decreasing with increasing temperature (and M_{Gar}). In general, garnet composition isopleths are almost horizontal (X_{Gar} is *T*-dependent) in the presence of one of the additional buffers and almost vertical (X_{Gar} is $X^{Al_2O_3}_{bulk-rock}$-dependent) in their absence (Fig. 5c, d).

'Typical' pelites lie towards the low Al_2O_3 end of the *x*-axes in Fig. 5 (the vertical dashed line at $x = 0.2$ represents $X^{Al_2O_3}_{bulk-rock} = 11.6$). In this range, X_{Gar} isopleths are vertical at temperatures above Par-out (*ca.* 620°C at 1.0 GPa) and garnet compositions are, therefore, expected to be strongly $X^{Al_2O_3}_{bulk-rock}$-dependent. This sensitivity to bulk-rock composition is reduced by plotting ratios of phase compositions. In the case of $[K_D]^{Mg}_{Fe\ Gar\ Bio}$ (Fig. 5e), a change in X^{alm}_{Gar} across any *PTX* point is associated with both compensation in X^{gro}_{Gar}, X^{pyr}_{Gar} and/or X^{spe}_{Gar} (unshown), and a corresponding change in the Fe/Mg content of biotite. For example, increasing $X^{Al_2O_3}_{bulk-rock}$ from 10 to 12% at 500°C and 1 GPa (i.e. from $x = 0.15$ to $x = 0.3$ in Fig. 5c) increases equilibrium X^{alm}_{Gar} from *ca.* 0.44–0.50 and X^{pyr}_{Gar} (not shown) from *ca.* 0.03 to 0.04. The result is a net

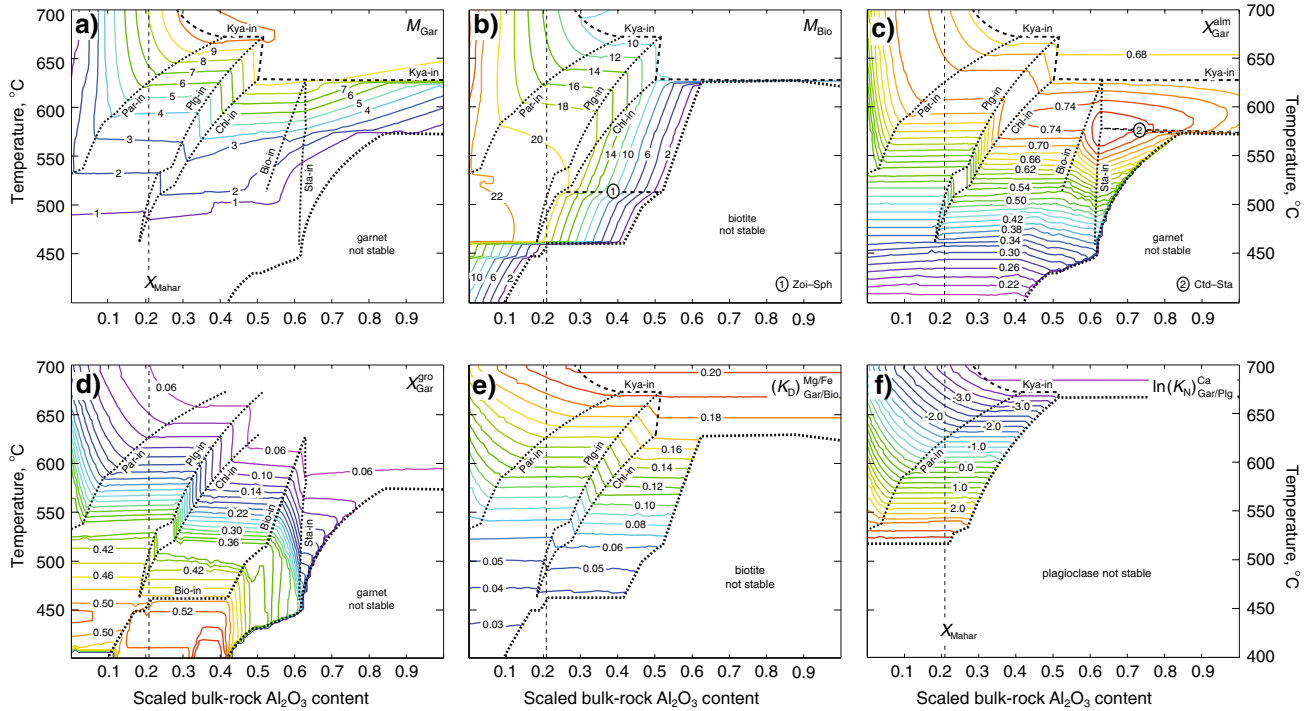

Fig. 5 The effect of varying bulk-rock Al_2O_3 content of a pelite on mineral modes and compositions, shown in $T - X^{Al_2O_3}_{bulk-rock}$ sections at $P = 1.0$ GPa. *Vertical dashed lines* indicate bulk composition used for Figs. 1, 2, 3 and 4 (11.6 mol% at $x = ca.$ 0.22), with the x-axis corresponding to Al_2O_3 variation (in molecular proportions) between 8.2% (at $x = 0$) and 22.0% (at $x = 1$). Relative proportions of all other components as in Figs. 1 and 2. Melt-bearing assemblages are not considered. Sections contoured for volume proportion Gar and Bio (**a**, **b**), almandine and grossular content of Gar (**c**, **d**), K_D of the Gar-Bio thermometer (**e**) and K_N of the Gar–Plg barometer (**f**), as defined in Fig. 2. *Dotted lines* indicate significant assemblage boundaries

$X^{pyr}_{Gar}/X^{alm}_{Gar}$ increase. Corresponding changes in biotite composition result in $X^{phl}_{Bio}/X^{ann}_{Bio}$ increase, with enhanced Mg-contents in both phases balanced by reduction in the modal proportion of biotite. Expressing K_D of the Gar–Bio exchange thermometer as the ratio between $X^{pyr}_{Gar}/X^{alm}_{Gar}$ and $X^{phl}_{Bio}/X^{ann}_{Bio}$ minimises this step, with $[K_D]^{Mg/Fe}_{Gar-Bio}$ varying from *ca.* 0.050 to 0.053 over this $X^{Al_2O_3}_{bulk-rock}$ range (Fig. 5e). Indeed, over a wide compositional range, $[K_D]^{Mg/Fe}_{Gar-Bio}$ is shown to be relatively insensitive to $X^{Al_2O_3}_{bulk-rock}$, highlighting its general utility as a thermometer. A $X^{Al_2O_3}_{bulk-rock}$ dependence is, however, evident at higher temperatures in low Al_2O_3 rocks.

$[K_N]^{Ca}_{Gar-Plg}$ isolines (Fig. 5f) show a simple $X^{Al_2O_3}_{bulk-rock}$-independent trend for compositions with sufficient Al to saturate either paragonite or kyanite. At lower $X^{Al_2O_3}_{bulk-rock}$, however, isolines are strongly bulk-rock composition dependent, demonstrating the importance of a fully buffered assemblage (e.g. kyanite and quartz bearing in GASP, Ghent 1976). The total variance of the 'buffered' fields in this case is 4 (components = 10 and phases = 8), with the loss of kyanite or paragonite increasing variance accordingly. High-Al bulk-rock compositions yield small Plg stability fields due to the enhanced stabilities of paragonitic mica and garnet. The range of bulk-rock compositions over which Gar–Plg barometers are applicable for low T rocks is thus limited by $X^{Al_2O_3}_{bulk-rock}$-dependent feldspar-in reactions.

CaO variation

Variation in CaO modifies the stability and compositions of garnet, plagioclase, and numerous calcic accessory phases. The effects of addition or subtraction of CaO from the average (Mahar et al. 1997) pelite composition at 1 GPa are shown in Fig. 6, with scaling of 0.1 mol% CaO at the left axis and 3.0% at the right.

Low temperature garnet compositions (Fig. 6a, b) are closely correlated with garnet abundance (unshown), showing little $X^{CaO}_{bulkrock}$ dependence other than in a small high-variance (Chl and Alb absent) field between *ca.* 470 and 550°C (Fig. 6a, b). Increasing variance with the loss of paragonite above *ca.* 560°C results in a negative correlation between bulk-rock CaO content and X^{alm}_{Gar}, and a

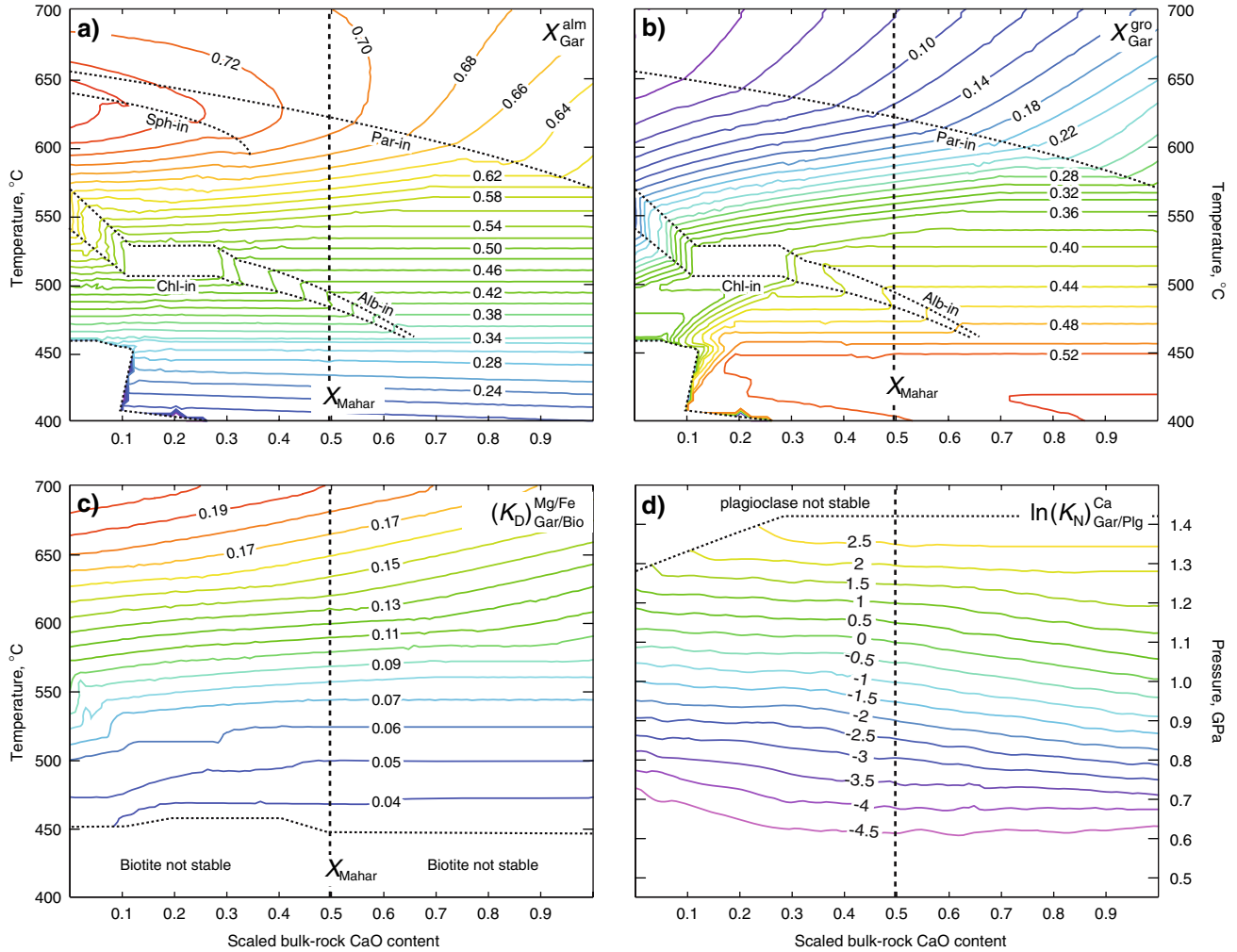

Fig. 6 The effect of varying bulk-rock CaO content of a pelite on mineral compositions, shown in isobaric sections (**a**–**c**) calculated at $P = 1.0$ GPa and an isothermal section (**d**) calculated at $T = 600$°C. *Vertical dashed lines* indicate the bulk composition used for Figs. 1 and 2, with the *x*-axis corresponding to CaO variation (in molecular proportions) between 0.1% (at $x = 0$) and 3.0% (at $x = 1$). Relative proportions of all other components as in Figs. 1 and 2. Melt-bearing assemblages are not shown. Sections contoured for garnet composition *X*, (**a**, **b**), K_D of the Gar-Bio thermometer (**c**) and K_N of the Gar–Plg barometer (**d**), as defined in Fig. 2. *Dotted lines* indicate significant assemblage boundaries

positive correlation with X_{Gar}^{gro}. Plagioclase composition (not shown) is simply correlated with bulk-rock Ca content, X_{Plg}^{ano} increasing linearly with increasing $X_{bulk-rock}^{CaO}$ over the examined *PTX* range.

$[K_D]_{Gar\ Bio}^{Mg\ Fe}$ isopleths are relatively $X_{bulk-rock}^{CaO}$-independent at all temperatures (Fig. 6c), but the compositional ratios still show a step associated with the high-variance (Chl and Alb absent) field between *ca*. 470 and 550°C. At $T > 550$°C, the dependence of $[K_D]_{Gar\ Bio}^{Mg\ Fe}$ on $X_{bulk-rock}^{CaO}$ is markedly less than that of individual phase compositions, although $[K_D]_{Gar\ Bio}^{Mg\ Fe}$ does decrease with increasing bulk-rock CaO in the absence of Par (Fig. 6c). For example, an isothermal (625°C), isobaric (1.0 GPa) section for the $X_{bulk-rock}^{CaO}$ range 0.1–3.0 mol% yields $[K_D]_{Gar\ Bio}^{Mg\ Fe}$ values between *ca*. 0.16 and 0.12. Recalculation with these values gives apparent temperatures of 644–612°C and 597–575°C with calibration (2) and the Hodges and Spear (1982) calibration, respectively. Although this appears to show a strong $[K_D]_{Gar\ Bio}^{Mg\ Fe}$ dependence on bulk-rock CaO we stress that the $X_{bulk-rock}^{CaO}$ bracket explored in Fig. 6 is wider than that of average pelitic rocks, which typically lie in the central third of the range and are thus subject to less $X_{bulk-rock}^{CaO}$-dependent $[K_D]_{Gar\ Bio}^{Mg\ Fe}$ variation.

Despite the dependence of garnet and plagioclase compositions on $X_{bulk-rock}^{CaO}$, the ratio $X_{Gar}^{gro} / X_{Plg}^{ano}$ is relatively

$X^{CaO}_{bulk-rock}$-independent (shown by a *PX*-section in Fig. 6d). For example, at 600°C, 1.0 GPa the explored $X^{CaO}_{bulk-rock}$ range yields $\ln[K_N]^{Ca}_{Gar\ Plg}$ values in the range −1.5 to 0, with most of the variation occurring at higher CaO content than the average bulk-rock explored in Figs. 1, 2, 3, and 4.

MnO variation

Figure 7 demonstrates the significance of a relatively minor component (MnO), with *x*-axis scaling between $X^{MnO}_{bulk-rock} = 0$ and 2 mol% MnO. Calculated M_{Gar} (Fig. 7a) is positively correlated with both bulk-rock MnO content and temperature. Strong Mn partitioning into garnet is clear, with a simple positive correlation between $X^{MnO}_{bulk-rock}$ and X^{spe}_{Gar} in most assemblage fields (Fig. 7b). Mn-rich bulk-rock compositions thus contain more garnet with higher spessartine contents than low-Mn rocks. No strong dependence of X^{alm}_{Gar} on bulk-rock Mn content is evident at low temperatures (Fig. 7c) although isopleths undergo a step associated with chlorite-out (which occurs at decreasing temperature for increasing $X^{MnO}_{bulk-rock}$). Above *ca.* 550°C, however, almandine and spessartine contents are inversely correlated and X^{alm}_{Gar} becomes increasingly $X^{MnO}_{bulk-rock}$ -dependent.

Despite the sensitivity of garnet and biotite (not shown) compositions to $X^{MnO}_{bulk-rock}$, calculated isopleths for $[K_D]^{Mg}_{Fe\ Gar\ Bio}$ (Fig. 7d) are almost completely independent of bulk-rock MnO content over a wide range of compositions. This

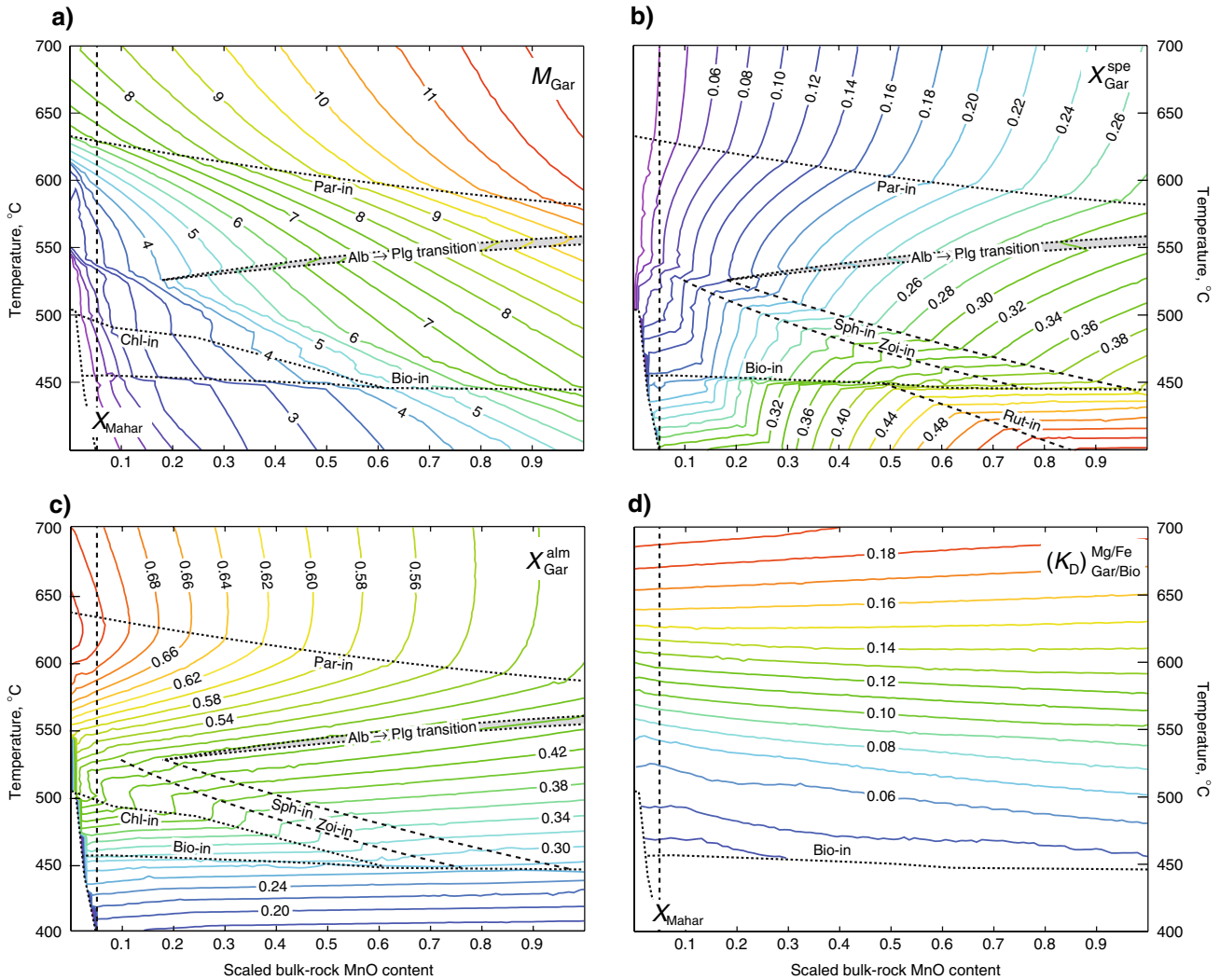

Fig. 7 The effect of varying bulk-rock MnO content of a pelite on mineral modes and compositions, shown in isobaric sections calculated at $P = 1.0$ GPa. *Vertical dashed lines* indicate the bulk composition used for Figs. 1 and 2, with the *x*-axis corresponding to MnO variation (in molecular proportions) between 0% (at $x = 0$) and 2% (at $x = 1$). Relative proportions of all other components as in Figs. 1 and 2. Melt-bearing assemblages are not considered. Sections contoured for modal proportion Gar (**a**), garnet composition (**b**, **c**), and $[K_D]^{Mg}_{Fe\ Gar\ Bio}$ (**d**). *Dotted lines* indicate significant assemblage boundaries

partly reflects the relative ideality of spessartine in the garnet solution model (we used a $W_{pyr,spe}$ value of 4.5 kJ mol^{-1} which is comparable to $W_{pyr,alm}$ [2.55 kJ mol^{-1}] and significantly smaller than the strongly non-ideal $W_{pyr,gro}$ [33 kJ mol^{-1}]) which does not modify the Fe/Mg ratio.

The complex relationships between a relatively minor component and the stabilities of phases that do not partition that component are also evident from Fig. 7. For example, sequestration of additional components (e.g. Ca, K, Si, Al and Ti) into Gar and Bio upon increasing $X^{MnO}_{bulk-rock}$ at $T < 500$°C reduces the modes of other phases requiring these elements. This is well demonstrated by the $X^{MnO}_{bulk-rock}$-dependent limits of rutile, chlorite, zoisite, and sphene stability.

When do mineral geothermobarometers reflect equilibrium conditions?

Our main interest in reliable mineral geothermobarometry is to reconstruct segments of metamorphic *PT* paths. Against the framework of our equilibrium calculations, we can assess whether disequilibrium features such as some mineral inclusions, chemically zoned crystals, or overgrowth textures give additional information about the deduced *PT* path or rather indicate that values recovered on the basis of chemical equilibrium must be reassessed.

Metamorphic rocks that maintain chemical equilibrium during changing *P* and *T* should continually adjust their mineralogy (mode, composition, and texture). Such rocks are typically presumed to preserve the mineralogy close to the peak temperature (such that deduced P_{Max} approximately coincides with T_{Max}), and in this framework no record of the prograde path would be preserved. Given, however, that zoned crystals record an attempt to maintain equilibrium under changing *PTX* conditions, simple inferences regarding points of equilibration can be made by comparing multiple crystals within a sample and multiple samples within a terrain. For example, different crystal rim compositions or zoning patterns of any given phase within a sample are indicative of incomplete specimen-scale equilibration during growth, asynchronous crystal growth, or both.

If cooling from T_{Max} is slow, partial re-equilibration is possible and would be recorded by modified zoning in porphyroblasts (Florence and Spear 1991). *P* recorded by slowly exhumed samples may thus not accurately reflect P_{Max}. Fortunately, evidence of compositional resetting associated with net-transfer reactions is detectable due to the formation of new phases and 'inverse' zoning in those phases that are partially resorbed (e.g. Kohn and Spear 2000). Fast exhumation tends to record *P* closer to maximum depth. Determining whether samples have experienced slow or fast exhumation is typically deduced from the behaviour of whole metamorphic terranes, partly from geochronology on multiple isotope and mineral systems, and partly from examining major and trace element mineral zoning within individual crystals. Calibrating exhumation rates usually requires isotopic systems and fission tracks that have lower effective-closure temperatures than the cations used for mineral geothermobarometry, so exhumation chronologies can record orogenic processes not well recorded by metamorphism, and vice versa.

It is clear that individual rocks maintaining equilibrium during heating (and then perhaps diverging from it during cooling) only give limited information about the entire *PT* path, and that further information should be obtained from sampling across entire terrains. For example, equilibrium samples collected across larger regions should show a geometrical relationship between sampling location and deduced pressure (and in some cases, temperature). However, this only applies if sampled terrains have been part of the same lithosphere fragment during the recorded part of the *PT* path and can be used to also reveal otherwise indiscernible juxtaposed fragments on the scale of tens of metres to tens of kilometres (e.g. Fraser et al. 2000). Deducing the recorded *PT* conditions across an entire exhumed metamorphic terrane (the metamorphic *PT* array of England and Richardson 1977) also provides thermal information about the setting (convergent, extensional or subduction), which can be compared with tectonic and stratigraphic records. Correlations between recorded *PT* datasets for numerous samples may also be used in an inverse way to calibrate rates of formation of the disequilibrium textures and compositions clearly produced in some terranes (e.g. Carlson 2003).

Rocks which have experienced several metamorphic events, as evidenced by overgrown mineral assemblages of quite different facies, require greatly detailed work to interpret overprinted records of diachronous *PT* histories. Furthermore, localised deformation can influence the ability of phases to record peak *PT* compositions (e.g. Steffen and Selverstone 2006). The study of multiple samples spanning an entire terrane, correlation of deformation phases, and use of absolute geochronologies from different parts of minerals (e.g. garnet core and rim dating; Argles et al. 1999) can resolve the lack of an obvious a priori way of distinguishing 'inherited' mineralogies.

Summary

Several mineral geothermobarometers for use in metapelitic rocks have been calibrated. These can be used for rocks experiencing large regions of *PT* space (0.1–3 GPa,

400–900°C), assuming attainment of local chemical equilibrium. Revisions to both end-member and solution model data will allow refinement of our *PTX* plots and thermobarometer calibrations, with all calculations being highly sensitive to both factors (Applegate and Hodges 1994; Holdaway 2001).

We emphasise that the plotting of single-mineral compositions on *PT* diagrams results in isoline sets that are appropriate only for restricted bulk-rock compositions close to that of the calibration. We advocate instead, direct plotting of equilibrium constants (K_D or K_N) that can be modified to deal with further chemical complexity by adding simple correction factors to the equilibrium expression. Figures 1, 2 and 4 can thus be used as templates to locate *PT* fields of equilibration simply on the basis of assemblage and coexisting mineral compositions.

Contrary to many previous studies (e.g. Thompson 1984), even iso-K_D lines for the well-known Gar–Bio Mg–Fe exchange thermometer are not necessarily straight and regularly spaced over large *PT* regions. This can lead to systematic deviation between actual and deduced temperature when using thermometers calibrated at or below 0.5 GPa (e.g. Ferry and Spear 1978) for rocks that equilibrated at pressures above the plagioclase–omphacite reactions. Indeed, our calibration of this thermometer (Eq. 2) is in good agreement with that of Ferry and Spear (1978) at low *P*, but deviates significantly from it as garnet compositions become grossular-rich (Appendix 2). Figures 5, 6, and 7 highlight the importance of the buffering assemblage, revealing that mineral compositions may be highly dependent on bulk-rock composition in parts of *PTX* space, but relatively insensitive to it in regions with adequately buffered assemblages. Furthermore, although K_D and K_N ratios are subject to less bulk-rock composition-dependence than absolute mineral compositions, they still require an adequate buffering assemblage. In practice, however, the buffering assemblage during growth may be difficult to assess, particularly if phases now exist only as stranded remnants of a prograde assemblage.

The disposition of large mineral assemblage fields separated by numerous smaller fields (Fig. 1) allows unusual or rare mineral assemblage occurences to be accurately located in *PT*-space without knowing mineral compositions in advance. This presents clear advantages when trying to locate *PT* paths for samples where parts of successively overprinted assemblages may be located as inclusions within later porphyroblasts. It is then straightforward to compare mineral modes, chemistries, and zoning patterns with isoline maps, presented here and in similar studies (e.g. Kelsey et al. 2003; Marmo et al. 2002; Storm and Spear 2005; Wei et al. 2003), which show the tendency for growth, dissolution or compositional change of phases as *PT* is changed. Against this background we can then begin to calibrate the disequilibrium features inherent in chemical zoning and incomplete mineral reactions. Subsequent refinement of the *PTt* paths reconstructed from detailed thermobarometry and in situ (spot) geochronology will continue to be an important evaluator of the effects of heat sources at particular depths in evolving orogens (be they convergent, extensional, subductional or combining elements of each).

Acknowledgments We would like to thank James Connolly for advice on and continued development of Perple_X. This work benefited particularly from discussion with James and Tim Holland. We thank two anonymous reviewers and our editor for helpful and insightful comments. This work is supported by ETH Research Funds.

Appendix 1: Activity-composition models and mineral abbreviations

The principle site occupancies permitted by the solution models used, and their source references are outlined here. Further details are available from the Perplex website of JAD Connolly (Table 2).[2]

Additional mineral abbreviations: Lawsonite (Law), rutile (Rut), zoisite (Zoi), sphene (Sph), sillimanite (Sil), andalusite (And), kyanite (Kya), quartz (Qtz), coesite (Coe), end-member albite (alb), anorthite (ano), almandine (alm), grossular (gro), pyrope (pyr), spessartine (spe), diopside (dio), phlogopite (phl), annite (ann).

Appendix 2: Comparing thermobarometer calibrations

The mineral thermobarometers calibrated in the text have been examined to show both how well the simple regressions model the composition data and how they compare with published thermobarometer calibrations. Firstly the minimum-free-energy phase compositions calculated as a function of *P* and *T* by Perplex were input to the thermobarometer calibrations and the predicted *PT*s plotted. For example, Gar–Bio calibration (2) yields *T* within 50°C of the 'expected' value over the entire examined *PT* range and within 15°C over most of that range (Fig. 8). The same composition data were also input to published thermobarometer calibrations, and the differences in predicted *P* or *T* between these calibrations and ours were calculated. For example, the difference between calibration (2) and the Gar–Bio calibration of Ferry and Spear (1978) is less than 15°C at pressures of *ca*. 5 kbars, increasing to over 200°C in extreme cases of high *P*, low *T* (Fig. 8). Finally, our

[2] http://www.perplex.ethz.ch/perplex/datafiles/newest_format_solut.dat

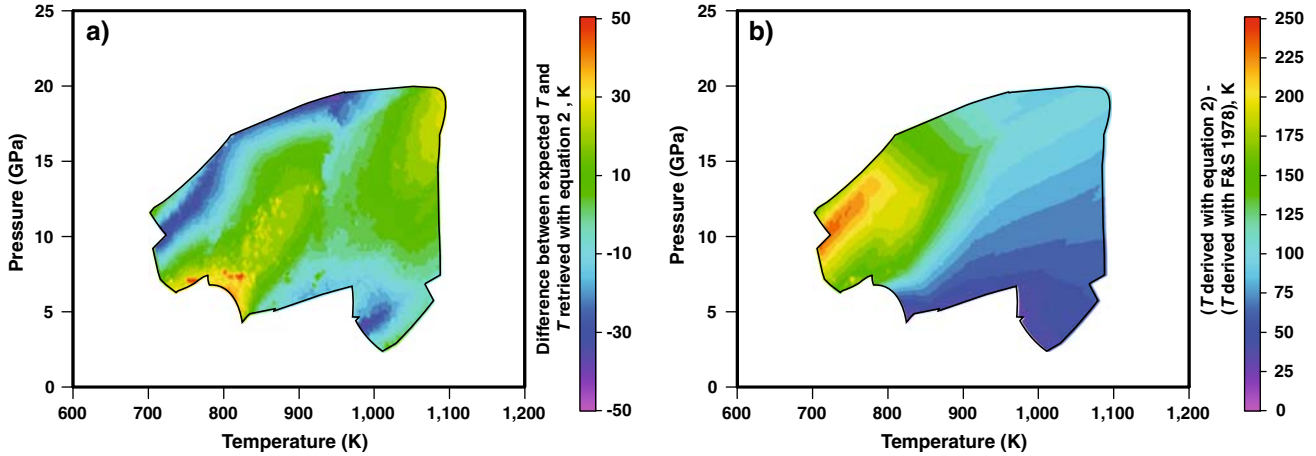

c)

Sample (Hodges & Spear, 1982)	78B	80D	90A	92D	145E	146B	146D
T, °C (This work, calibration 2)	510	540	526	532	538	559	507
T, °C (Ferry & Spear, 1978)	468	496	486	492	500	522	467
T, °C (Hodges and Spear, 1982)	478	517	498	500	507	537	482
T, °C (Perchuk and Lavrent'eva, 1983)	518	535	529	533	538	551	518
T, °C (Thompson, 1976)	502	526	518	522	529	547	502
T, °C (Holdaway & Lee, 1977)	500	521	513	518	524	539	499

Fig. 8 **a** Plot of the difference between T at which mineral compositions are output by free energy minimisation (Perplex) and T derived using Eq. 2 and those phase compositions. **b** Difference between T derived using Eq. 2 and the Ferry and Spear (1978) geothermometer, both with input phase compostions as in **a**. **c** Comparison with 5 alternative geothermometers using mineral compositions from Hodges and Spear (1982) and an assumed P of 0.376 GPa

Table 2 Activity-composition models and mineral abbreviations

Phase (abbreviation)	Model geometry and permitted site occupancies	Source
Biotite (Bio)	*Symmetric*. **M1** (Ti, Al, Mn, Fe, Mg); **M2** (Mn□, Fe□, Mg□, 2Mn, 2Mg, 2Fe); **T1** (AlSi, AlAl)	White et al. (2000)
Garnet (Gar)	*Symmetric*. **M** $(Fe, Mg, Ca, Mn)_3$	Powell and Holland (2001)
Chlorite (Chl)	*Symmetric*. **M1** (Al, Mn, Fe); **M2/M3** $(Mn, Fe, Mg)_4$; **M4** (Al, Mn, Fe, Mg); **T2** (AlAl, AlSi, SiSi)	Based on Holland et al. (1998)
Staurolite (Sta)	*Symmetric*. **M** $(Mg, Fe, Mn)_4$	Based on Mahar et al. (1997)
White mica (Mus, Phe or Par)	*Van Laar*. **A** (K, Na, Ca); **M2** (Al, Mg, Fe); **T1** (AlAl, AlSi, SiSi)	Coggon and Holland (2002)
Amphibole (Amp)	*Van Laar*. **A** (Na, □); **M13** $(Mg, Fe)_3$; **M2** (2Mg, 2Fe, 2Al, MgAl, FeAl); **M4** $(Ca, Na)_2$; **T1** $(SiSi, AlSi)_2$	Dale et al. (2005)
Feldspar (Plg or Kfs)	*Symmetric*. **A** (Ca, Na, K); **T1** (SiSi, AlSi)	Furman and Linsley (1988)
Omphacite (Omp or Cpx)	*Symmetric*. **M2a** $(Ca, Na)_{0.5}$; **M2b** $(Ca, Na)_{0.5}$; **M2a** $(Mg, Fe, Al)_{0.5}$; **M2b** $(Mg, Fe, Al)_{0.5}$	Based on Holland and Powell (1996)
Cordierite (Crd)	*Symmetric*.**M2**$(Mn, Fe, Mg)_2$;**H**$(□, H_2O)$	Mahar et al. (1997)
Chloritoid (Ctd)	*Symmetric*. **M** (Mn, Fe, Mg)	Based on Mahar et al. (1997)
Orthopyroxene (Opx)	*Symmetric*. **M1** (Fe, Mg, Al); **M2** (Fe, Mg); **T** (AlSi, SiSi)	Powell and Holland (1999)
Ilmenite (Ilm)	*Ideal*. **M** (Mg, Fe, Mn)	
Melt (Liq)	*Symmetric* mixing of albite, anorthite, K-feldspar, quartz, sillimanite, forsterite, fayalite and water melt-end-members, with mixing of the 'mineral' end-members on an 8 oxygen unit basis	White et al. (2001)

calibrations have been compared to others from the literature using experimentally derived phase compositions or those from well-studied natural samples. For example, the seven Mt. Moosilauke compositions of Hodges and Spear (1982) yield temperatures of 477–538°C with the Hodges and Spear thermometer (assumed $P = 0.376$ GPa and $W_{MgMn} = 0$) and 507–559°C with our calibration (2) (Fig. 8). Similar plots and descriptions are available for each of the calibrated thermobarometers as electronic supplemental material.

References

Applegate JDR, Hodges KV (1994) Empirical evaluation of solution models for pelitic minerals and their application to thermobarometry. Contrib Mineral Petrol 117:56–65

Argles TW, Prince CI, Foster GL, Vance D (1999) New garnets for old? Cautionary tales from young mountain belts. Earth Planet Sci Lett 172:301–309

Caddick MJ, Bickle MJ, Harris NBW (2004) Early exhumation of the High Himalayas in the absence of melt? *PTt* path constraints from the eastern and western Himalaya In: Channel flow, ductile extrusion and exhumation of lower-mid crust in continental collision zones; Abstract volume, Geological Society of London, UK, p 5

Caddick MJ, Bickle MJ, Harris NBW, Holland TJB, Horstwood MSA, Ahmad T (2007) Burial and exhumation history of a Lesser Himalayan schist: recording the formation of an inverted metamorphic sequence in NW India. Earth Planet Sci Lett 264(3–4):375–390

Carlson WD (2003) Constraints on diffusion rates in garnet from natural occurrences. Geochim Cosmoschim Acta 67(18):A52–A52

Coggon R, Holland TJB (2002) Mixing properties of muscovite-celadonite-ferroceladonite-paragonite micas and revised garnet-phengite thermobarometers. J Metamorph Geol 20(7):683–696

Connolly JAD (1990) Multivariable phase diagrams: an algorithm based on generalized thermodynamics. Am J Sci 290:666–718

Connolly JAD (2005) Computation of phase equilibria by linear programming: a tool for geodynamic modeling and its application to subduction zone decarbonation. Earth Planet Sci Lett 236:524–541

Connolly JAD, Kerrick DM (1987) An algorithm and computer program for calculating composition phase diagrams. Comput Geosci 11:1–55

Dale J, Powell R, White RW, Elmer FL, Holland TJB (2005) A thermodynamic model for Ca–Na clinoamphiboles in $Na_2O - CaO - FeO - MgO - Al_2O_3 - SiO_2 - H_2O - O$ J Metamorph Geol 23:771–791

Ellis DJ, Green DH (1979) An experimental study of the effect of Ca upon Garnet-Clinopyroxene Fe–Mg exchange equilibria. Contrib Mineral Petrol 71:13–22

England PC, Holland TJB (1979) Archimedes and the Tauern eclogites: the role of buoyancy in the preservation of exotic eclogite blocks. Earth Planet Sci Lett 44:287–294

England PC, Richardson SW (1977) The influence of erosion upon the mineral facies of rocks from different metamorphic environments. J Geol Soc 134:201–213

England PC, Thompson AB (1984) Pressure–temperature–time paths of regional metamorphism I. Heat transfer during the evolution of regions of thickened continental crust. J Petrol 25:894–928

Ernst WG (2006) Preservation/exhumation of ultrahigh-pressure subduction complexes. Lithos 92:321–335

Ferry JM, Spear FS (1978) Experimental calibration of the partitioning of Fe and Mg between biotite and garnet. Contrib Mineral Petrol 66:113–117

Florence FP, Spear FS (1991) Effects of diffusional modification of garnet growth zoning on P-T path calculations. Contrib Mineral Petrol 107:487–500

Fraser G, Worley B, Sandiford M (2000) High-precision geothermobarometry across the High Himalayan metamorphic sequence, Langtang Valley, Nepal. J Metamorph Geol 18:665–681

Furman ML, Lindsley DH (1988) Ternary feldspar modeling and thermometry. Am Miner 73:201–215

Gardien V, Thompson AB, Grujic D, Ulmer P (1995) Experimental melting of biotite + plagioclase + quartz ± muscovite assemblages and implications for crustal melting. J Geophys Res 100(B8):15581–15591

Ghent ED (1976) Plagioclase–garnet–Al_2SiO_5–quartz: a potential geothermometer–geobarometer. Am Miner 61:710–714

Ghent ED (1977) Applications of activity-composition relations to displacement of a solid–solid equilibrium anorthite = grossular + kyanite + quartz. In: Greenwood HJ (ed) Short course in application of thermodynamics to petrology and ore deposits, vol 2. Mineralogical Association of Canada

Green TH, Hellman PL (1982) Fe–Mg partitioning between coexisting garnet and phengite at high pressure, and comments on a garnet-phengite geothermometer. Lithos 15:253–266

Hacker BR, Ratschbacher L, Webb L, Shuwen D (1995) What brought them up? Exhumation of the Dabie Shan ultrahigh-pressure rocks. Geology 23(8):743–746

Harris NBW, Caddick MJ, Kosler J, Goswami S, Vance D, Tindle AG (2004) The pressure–temperature-time path of migmatites from the Sikkim Himalaya. J Metamorph Geol 22:249–264

Hodges KV, Spear FS (1982) Geothermometry, geobarometry and the Al_2SiO_5 triple point at Mt. Moosilauke, New Hampshire. Am Miner 67:1118–1134

Holdaway MJ (2001) Recalibration of the GASP geobarometer in light of recent garnet and plagioclase activity models and versions of the garnet-biotite geothermometer. Am Miner 86:1117–1129

Holdaway MJ, Lee SM (1977) Fe–Mg cordierite stability in high-grade pelitic rocks based on experimental, theoretical, and natural observations. Contrib Mineral Petrol 63:25–43

Holland TJB (1980) The reaction albite = jadeite + quartz determined experimentally in the range 600–1200°C. Am Miner 65:129–134

Holland TJB, Powell R (1996) Thermodynamics of order–disorder in minerals: II. Symmetric formalism applied to solid solutions. Am Miner 81:1425–1437

Holland TJB, Powell R (1998) An internally consistent thermodynamic data set for phases of petrological interest. J Metamorph Geol 16:309–343

Holland TJB, Powell R (2001) Calculation of phase relations involving hapologranitic melts using an internally consistent thermodynamic dataset. J Petrol 42:673–683

Holland TJB, Baker J, Powell R (1998) Mixing properties and activity-composition relationships of chlorites in the system $MgO - FeO - Al_2O_3 - SiO_2 - H_2O$ Euro J Mineral 10:395–406

Huang WL, Wyllie PJ (1973) Melting relations of muscovite-granite to 35 kbar as a model for fusion of metamorphosed subducted oceanic sediments. Contrib Mineral Petrol 42:1–14

Johannes W, Chipman DW, Hays JF, Bell PM, Mao HK, Newton RC, Boettcher AL, Seifert F (1971) An interlaboratory comparison of piston-cylinder pressure calibration using the albite-breakdown reaction. Contrib Mineral Petrol 32:24–38

Kelsey DE, White RW, Powell R, Wilson CJL, Quinn CD (2003) New constraints on metamorphism in the Rauer Group, Prydz Bay, east Antarctica. J Metamorph Geol 21:739–759

Kohn MJ, Spear FS (2000) Retrograde net transfer reaction insurance for pressure–temperature estimates. Geology 28:1127–1130

Kriegsman LM (2001) Partial melting, partial melt extraction and partial back reaction in anatectic migmatites. Lithos 56:75–96

Mahar E, Powell R, Holland TJB, Howell N (1997) The effect of Mn on mineral stability in metapelites. J Metamorph Geol 15(2):223–238

Marmo BA, Clarke GL, Powell R (2002) Fractionation of bulk rock composition due to porphyroblast growth: effects on eclogite facies mineral equilibria, Pam Peninsula, New Caledonia. J Metamorph Geol 20:151–165

Maruyama S, Liou JG, Zhang R (1994) Tectonic evolution of the ultrahigh-pressure (UHP) and high-pressure (HP) metamorphic belts from central China. Island Arc 3:112–121

Massonne HJ, Schreyer W (1987) Phengite geobarometry based on the limiting assemblage wth K-feldspar, phlogopite, and quartz. Contrib Mineral Petrol 96:212–224

Massonne HJ, Szpurka Z (1997) Thermodynamic properties of white micas on the basis of high-pressure experiments in the systems $K_2O - MgO - Al_2O_3 - SiO_2 - H_2O$ and $K_2O - FeO - Al_2O_3 - SiO_2 - H_2O$ Lithos 41:229–250

Newton RC, Haselton HT (1981) Thermodynamics of the garnet-plagioclase-Al_2SiO_5-quartz geobarometer. In: Newton RC, Navrotsky A, Wood BJ (eds) Thermodynamics of minerals and melts, vol 1. Springer, Berlin

Newton RC, Smith JV (1967) Investigations concerning the breakdown of albite at depth in the Earth. J Geol 75:268–286

Okay AI, Sengör AMC, Satir M (1993) Tectonics of an ultrahigh-pressure metamorphic terrane: The Dabie Shan/Tongbai Shan orogen, China. Tectonics 12:1320–1334

Perchuk LL, Lavrent'eva IV (1983) Experimental investigation of exchange equilibria in the system cordierite–garnet–biotite. In: Saxena SK (ed) Kinetics and equilibrium in mineral reactions, vol 3. Springer, New York, pp 199–239

Powell R, Holland TJB (1990) Calculated mineral equilibria in the pelite system, KFMASH $K_2O - FeO - MgO - Al_2O_3 - SiO_2 - H_2O$ Am Miner 75:367–380

Powell R, Holland TJB (1993) On the formulation of simple mixing models for complex phases. Am Miner 78:1174–1180

Powell R, Holland TJB (1999) Relating formulations of the thermodynamics of mineral solid solutions: activity modeling of pyroxenes, amphiboles, and micas. Am Miner 84:1–14

Powell R, Holland TJB (2001) Course notes for "THERMOCALC workshop 2001: Calculating metamorphic phase equilibria"

Powell R, Holland TJB, Worley B (1998) Calculating phase diagrams involving solid solutions via non-linear equations, with examples using THERMOCALC. J Metamorph Geol 16(4):577–588

Ravna EK (2000) The garnet-clinopyroxene $Fe^{2+} - Mg$ geothermometer: an updated calibration. J Metamorph Geol 18:211–219

Rubatto D, Hermann J (2001) Exhumation as fast as subduction? Geology 29(1):3–6

Saxena SK (1969) Silicate solid solutions and geothermometry: 3. Distribution of Fe and Mg between coexisting garnet and biotite. Contrib Mineral Petrol 22:259–267

Shaw DM (1956) Geochemistry of pelitic rocks. Part iii: major elements and general geochemistry. Bull Geol Soc Am 67:919–934

Spear FS, Cheney JT (1989) A petrogenetic grid for pelitic systems in the system $SiO_2 - Al_2O_3 - FeO - MgO - K_2O - H_2O$ Contrib Mineral Petrol 101:149–164

Spear FS, Selverstone J, Hickmott D, Crowley PD, Hodges KV (1984) P-T paths from garnet zoning—a new technique for deciphering tectonic processes in crystalline terranes. Geology 12(2):87–90

Steffen KJ, Selverstone J (2006) Retrieval of P–T information from shear zones: thermobarometric consequences of changes in plagioclase deformation mechanisms. Contrib Mineral Petrol 151:600–614

Storm LC, Spear FS (2005) Pressure, temperature and cooling rates of granulite facies migmatitic pelites from the southern Adirondack Highlands, New York. J Metamorph Geol 23:107–130

Storre B, Karotke E (1972) Experimental data on melting reactions of muscovite + quartz in the system $K_2O - Al_2O_3 - SiO_2 - H_2O$ to 20 Kb water pressure. Contrib Mineral Petrol 36:343–345

Symmes GH, Ferry JM (1991) Evidence from mineral assemblages for infiltration of pelitic schists by aqueous fluids during metamorphism. Contrib Mineral Petrol 108:419–438

Thompson JB (1957) The graphical analysis of mineral assemblages in pelitic schists. Am Miner 42:842–858

Thompson AB (1976) Mineral reactions in pelitic rocks: II. Calculation of some P–T–X (Fe–Mg) phase relations. Am J Sci 276:425–454

Thompson AB (1984) Mineral reactions and mineral equilibria and their use in geothermometry, geobarometry and geohygrometry. In: Lagache M (ed) Thermométrie et barométrie géologiques, vol. Société Française de Minéralogie et de Cristallographie, Paris, pp 179–199

Tracy RJ, Robinson P, Thompson AB (1976) Garnet composition and zoning in the determination of temperature and pressure of metamorphism, central Massachusetts. Am Miner 61:762–775

Vannay JC, Grasemann B (1998) Inverted metamorphism in the High Himalaya of Himachal Pradesh (NW India): phase equilibria versus thermobarometry. Schweiz Mineral Petrog Mitt 78:107–132

Waters DJ, Martin HN (1993) Geobarometry in phengite-bearing eclogites. Terra Abstr 5:410–411

Wei CJ, Powell R (2003) Phase relations in high-pressure metapelites in the system KFMASH ($K_2O - FeO - MgO - Al_2O_3 - SiO_2 - H_2O$) with application to natural rocks. Contrib Mineral Petrol 145:301–315

Wei CJ, Powell R (2004) Calculated phase relations in high-pressure metapelites in the system NKFMASH ($Na_2O - K_2O - FeO - MgO - Al_2O_3 - SiO_2 - H_2O$. J Petrol 45(1):183–202

Wei CJ, Powell R, Zhang LF (2003) Eclogites from the south Tianshan, NW China: petrological characteristic and calculated mineral equilibria in the $Na_2O - CaO - FeO - MgO - Al_2O_3 - SiO_2 - H_2O$ system. J Metamorph Geol 21:163–179

White RW, Powell R, Holland TJB, Worley B (2000) The effect of TiO_2 and Fe_2O_3 on metapelitic assemblages at greenschist and amphibolite facies conditions: mineral equilibria calculations in the system $K_2O - FeO - MgO - Al_2O_3 - SiO_2 - H_2O - TiO_2 - Fe_2O_3$ J Metamorph Geol 18(5):497–511

White RW, Powell R, Holland TJB (2001) Calculation of partial melting equilibria in the system $Na_2O - CaO - K_2O - FeO - MgO - Al_2O_3 - SiO_2 - H_2O$ (NCKFMASH). J Metamorph Geol 19:139–153

Wu C-M, Wang X-S, Yang C-H, Geng Y-S, Liu F-L (2002) Empirical garnet—muscovite geothermometry in metapelites. Lithos 62:1–13

Xu GW, Will TM, Powell R (1994) A calculated petrogenetic grid for the system $K_2O - FeO - MgO - Al_2O_3 - SiO_2 - H_2O$, with particular reference to contact metamorphosed pelites. J Metamorph Geol 12:99–119

Zeh A, Klemd R, Barton JM (2005) Petrological evolution in the roof of the high-grade metamorphic Central Zone of the Limpopo Belt, South Africa. Geol Mag 142(2):229–240